NASA TN D-1954

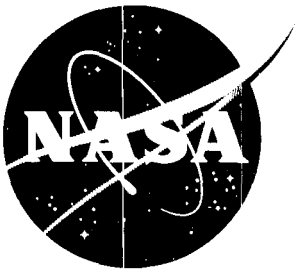

TECHNICAL NOTE

D-1954

PRESSURE DISTRIBUTIONS ON

BLUNT DELTA WINGS AT ANGLES OF ATTACK UP TO 90°

AND MACH NUMBER OF 6.85

By Peter T. Bernot

Langley Research Center
Langley Station, Hampton, Va.

NATIONAL AERONAUTICS AND SPACE ADMINISTRATION

WASHINGTON

July 1963

NATIONAL AERONAUTICS AND SPACE ADMINISTRATION

TECHNICAL NOTE D-1954

PRESSURE DISTRIBUTIONS ON BLUNT DELTA WINGS AT ANGLES OF ATTACK UP TO 90° AND MACH NUMBER OF 6.85

By Peter T. Bernot

SUMMARY

Pressure distributions were obtained on four blunt delta-wing models having sweep angles of 50°, 70°, 75°, and 80° over an angle-of-attack range from 30° to 90° and at a Mach number of 6.85.

In general, the pressures on the windward slab surfaces are constant for angles of attack up to about 50°. As angle of attack is increased further, pressure gradients occur on both the windward slab and leading-edge surfaces. Pressures on the windward leading edges decreased as distance from the wing apex increased, with significant pressure gradients occurring in the angle-of-attack range from 50° to 90°. Modified Newtonian theory yielded only fair agreement with the measured pressures. Effect of wing sweep angle is to raise the pressure level with decreasing sweep but this trend diminishes at angles of attack greater than 60°. The effect of angle of attack is best characterized by the fact that 90 percent of the maximum pressure rise is attained at an angle of attack of 70°. The measured pressures on the model center line are bracketed by the five-term hypersonic approximation and modified Newtonian theory. The proposed method of NASA Technical Memorandum X-757 shows fairly good agreement with the measured data.

INTRODUCTION

The advantages of lift control on reentering the atmosphere by a manned space vehicle are well known. Many investigations have been performed on winged reentry vehicles, several of which have basically a delta planform and are required to operate at high angles of attack. (See refs. 1 to 3.) Consequently, there is current interest in the aerodynamic characteristics of delta wings at angles of attack up to 90° over the flight Mach number range.

The purpose of this investigation was to provide hypersonic pressure distributions on several blunt delta wings having various sweep angles for an angle-of-attack range from 30° to 90°. The tests were performed at a Mach number of 6.85

and a unit Reynolds number of 270,000 per inch. These data should provide needed information on pressure loadings on delta wings and some insight into flow behavior. A comparison of the experimental data with several hypersonic theories was also made and assessed.

SYMBOLS

C_p pressure coefficient, $\frac{p - p_\infty}{\frac{\gamma}{2} M^2 p_\infty}$

l distance along leading edge measured from wing apex (fig. 1)

M free-stream Mach number

p pressure

s distance along surface normal to leading edge (fig. 1)

t wing thickness

α angle of attack

γ ratio of specific heats

Λ wing sweep angle

Subscripts:

t stagnation value behind normal shock

∞ free stream

APPARATUS, MODELS, AND TESTS

Facility

This investigation was conducted in the Langley 11-inch hypersonic tunnel, which is a blowdown-to-vacuum type. A two-dimensional, contoured nozzle fabricated from invar was used to produce a Mach number slightly under 7. In order to avoid liquefaction, dry air is passed through an electrically heated bundle of Nichrome tubes. A more detailed description of the tunnel and nozzle calibration data may be found in references 4 and 5. Model pressures were obtained on six-cell bellows-type instruments. Movement of the bellows was converted into rotation of a small mirror which reflected a beam of light onto a moving film and thereby provided a time history of the measured pressure. Stagnation temperature was measured by using chromel-alumel thermocouple wire whose output was recorded on a strip-chart potentiometer. Stagnation pressure was determined visually by

means of a face-dial gage. The tunnel facility is equipped with a schlieren system that has a vertical Z-shape light path in conjunction with a horizontal knife edge.

Models

The four test models were fabricated from stainless steel. In order to allow installation of the steel tubing, the wing models were built in halves, split symmetrically along a plane parallel to the slab surfaces. All models had sharp noses with hemicylindrical leading edges, and the trailing edges were straight with sharp corners. As shown in figure 1, the sweep angles were 50°, 70°, 75° and 80° with a design thickness of 0.375 inch for all models. Based on previous tunnel experience on flow choking, the planform area of these models did not exceed 5.5 square inches nor did the models have any dimension greater than 4.5 inches. For the windward slab and curved leading edges, the pressure orifice size was 0.040 inch; whereas, for the leeward surfaces, the orifice size was 0.060 inch. Orifice locations were positioned on lines normal to the leading edges, as shown in table I. In order to cover the angle-of-attack range, either a straight or a bent sting was employed. A photograph of a typical test model with the straight sting attached is shown in figure 2.

Tests

Average stagnation pressure and temperature conditions for these tests were 24.5 atmospheres absolute and 655° F, resulting in a Reynolds number of 270,000 per inch at a Mach number of 6.85. Data were obtained for one setting of angle of attack for each run, which had a duration of about 1 minute. The angle-of-attack range of this investigation was from 30° to 90° with data recorded for each 5° increment. Schlieren photographs were taken by using the flash technique during all runs. Surface flow patterns were obtained by use of the oil-flow technique. In this method, a mixture of lubricating oil and carbon black is applied to the model surface in a dot pattern by using a pointed instrument. The model is then subjected to the airstream for several seconds.

PRECISION OF DATA

In order to obtain optimum data accuracy, pressure instruments were selected as close as possible to full-scale deflections. The instruments available for these tests had full-scale pressures of 30, 10, and 0.8 inches of mercury absolute and the maximum estimates of uncertainties for the pressure coefficients are ±0.046, ±0.015, and ±0.001, respectively. Variation in Mach number was ±0.01 and maximum error for model angle of attack was ±0.10°. For the stagnation pressure used in these tests, the maximum error was ±2.5 inches of mercury. It is not known if the orifice size on the curved leading edges produced any additional data inaccuracies during this investigation. For example, the 0.040-inch orifice subtended an angle of about 12° whereas the 0.060-inch orifice subtended an angle of about 19°.

RESULTS AND DISCUSSION

General

The pressure-distribution curves in this paper are presented as the ratio p/p_t plotted against s/t. The value of p_t is taken as the ideal stagnation pressure behind the normal shock for the free-stream Mach number of 6.85. The measured pressure data, obtained at angle-of-attack increments of 5°, are tabulated in table I in coefficient form. The plotted results are presented for 10° increments. Positive values of the parameter s/t indicate the windward side of the models, with $s/t = 0$ being taken as the geometric stagnation point on the curved leading edges when the model is at an angle of attack of 0°. (See fig. 1.)

Schlieren photographs of the four test models over the angle-of-attack range are presented in figure 3.

Basic Plots

The complete pressure distributions on the four test models are presented in the basic plots of figure 4 for all the l/t stations over the angle-of-attack range of this investigation. From an overall standpoint, it can be stated that the pressures over the entire windward slab surfaces are a function of angle of attack and are generally constant for angles of attack up to about 50°. This effect is expected since the schlieren photographs of figure 3 reveal an essentially straight bow shock over this angle-of-attack range. As angle of attack is increased (from $\alpha = 50^\circ$ to $\alpha = 80^\circ$), further pressure gradients occur over these surfaces starting near the juncture of the curved leading edges and flat (slab) surfaces ($s/t = 0.785$) and gradually extending inboard. Examination of the schlieren photographs of figure 3 reveals that the bow shock becomes curved at an angle of attack near 60°; consequently, strong entropy and pressure gradients must exist in the flow. At angle of attack of 90°, the pressures become essentially constant again.

Another interesting characteristic to be noted from figure 4 is the effect of the distance from the wing apex (l/t) on the pressure levels. For the windward surfaces on the curved leading edges, it is seen that the pressure levels decrease with increasing values of l/t. This effect becomes prominent at an angle of attack of 50° for the four models and indicates that pressure relief through a bleed-off mechanism is occurring within the shock envelope. In general, this l/t effect is seen to extend up to the highest test angle of attack. Similar l/t effects are noted on the slab surface, except at an angle of attack of 90° where, as previously noted, the pressures become essentially constant, that is, independent of l/t. In reference 6, a method based on three-dimensional cross flow has been developed for predicting surface pressure distribution and flow streamlines on delta-wing planforms at an angle of attack of 90°. Reference 6 also shows that the isobars on a 70° sweep flat delta wing at an angle of attack of 90° and at a Mach number of 6.9 are generally parallel to the wing leading edges. Hence, the pressures are independent of l/t. Close inspection of the data for the windward leading edges, at an angle of attack of 90°, shows that the

l/t effect is more predominant for the 80° and 75° sweep models than for the 70° and 50° sweep models. The reason for this trend is not known but a sweep effect is indicated.

In general, the pressures on the leeward side of the four models are constant and usually in the neighborhood of free-stream static pressure. At a Mach number of 6.85, the measured pressure when equal to the free-stream static pressure yields a value of 0.0164 for p/p_t.

Modified Newtonian theory as presented in reference 7 was employed to estimate the pressure distributions on the four test models and is also indicated in figure 4. As suggested in reference 7, a value for C_p at the stagnation point was calculated from the following equation taken from reference 8:

$$C_{p,t} = \frac{\gamma + 3}{\gamma + 1}\left(1 - \frac{2}{\gamma + 3}\frac{1}{M^2}\right) \tag{1}$$

Comparison of theoretical and experimental results shows that for the slab windward surfaces, theory underpredicts the data at angles of attack up to 60°. However, theory is seen to give better agreement at the higher angles of attack. For the windward curved leading edges, theory has a tendency to overpredict the measured data at angles of attack from 60° to 90°. At the lower angles, however, the agreement is fairly good. On an overall basis, modified Newtonian theory yielded fair results and further refinements will be necessary for more accurate prediction of surface pressure on delta-wing models at hypersonic speed. For instance, the effect of l/t on the curved-leading-edge pressures is one significant parameter that merits further investigation.

Effect of Wing Sweep Angle

The effects of wing sweep angle on the pressure distributions of the four test models are presented in figure 5 over an angle-of-attack range from 40° to 90°. Since the values of l/t differed to some extent for all the models, a small spread of the l/t values is noted for each plot. The conclusions drawn from these resulting plots are believed to be valid. In general, the data indicate that for angles of attack up to 60°, the pressure levels are progressively higher as sweep angle is decreased. This effect is seen to occur over the windward slab and curved leading-edge surfaces. Varying the sweep angle has a negligible effect on the pressure levels for the leeward model surfaces, as might be expected. At angles of attack greater than 60°, varying the sweep angle does not have any significant effect on the pressure levels for the windward surfaces.

Effect of Angle of Attack

Figure 6 presents the pressure distributions on the test models for three l/t stations and shows the effects of angle of attack over the entire range of these tests. For the windward slab surfaces, the pressure levels are seen to increase with increasing angle of attack, as expected. More noteworthy is the fact that the pressure increments are quite substantial for angles of attack up

to 70° for all the test models. Over 90 percent of the maximum pressure rise is attained at an angle of attack of 70°. As angle of attack is increased further, these pressure increments are much smaller and are generally less than 10 percent of the pressure obtained at an angle of attack of 70°.

A different picture is evident for the pressure distributions on the windward leading-edge surfaces. The pressure increments are smaller over the entire angle-of-attack range for s/t values of 0 to about 0.52. Also, for this same s/t range and for the models having sweep angles of 50°, 70°, and 75°, the pressure levels are seen to decrease with increasing angle of attack. This trend is a reversal from that obtained over the slab surfaces. The reason for this trend, as stated in reference 9, can be ascribed, intuitively, to the geometry of the wing leading edge and its angle of exposure to the local flow direction. As shown in figure 6, the reversal effect is magnified as wing sweep angle is decreased.

Center-Line Pressures

A compilation of windward center-line chordwise pressures expressed in coefficient form is presented in figure 7 for the four test models over the angle-of-attack range. All the models had three orifices on the center line except the 50° sweep model, which had four. (See table I.) Although more orifices would have been desirable, it is believed that the measured data as presented herein would be of interest. As plotted, the test-point symbols represent the experimental values of pressure coefficient measured at the orifices nearest the middle. The range of pressures on the center line measured by the remaining orifices are also indicated in the figure by the short-line segments. For comparison, simple and modified Newtonian theories are presented. The value of $C_{p,t}$ is equal to 2.0 for the simple Newtonian theory. For the modified Newtonian theory, the value of $C_{p,t}$ was calculated from equation (1) and is equal to 1.815 for $M = 6.85$. Also shown are the results from a five-term hypersonic approximation (ref. 9) and from a method presented in a more recent publication (ref. 10).

Simple Newtonian theory gives good results for the models having sweep angles of 75° and 80° up to angles of attack of about 65°. For all four models, modified Newtonian theory yields pressure-coefficient values which are lower than the measured values except at angles of attack from about 75° to 90°, where reasonable agreement is indicated. This theory can be assumed as a lower limit for delta-wing center-line pressures as sweep angle is increased. In reference 11, pressure distributions on a circular cylinder, which can be likened to a delta wing of 90° sweep, show very good agreement with modified Newtonian theory at a Mach number of 6.86. In the present tests, the trend of the measured center-line pressures with increasing sweep angle indicates agreement with this estimation. As is evident from figure 7, Newtonian concepts are not completely adequate for predicting the pressure distribution for the model sweep angles and angle-of-attack range of this investigation.

The five-term hypersonic approximation is seen to overpredict the measured pressure coefficients at angles of attack up to about 70° for those models having sweep angles of 70° or greater. This result is expected since this approximation

is derived mainly for moderately swept wings. Accordingly, better agreement is noted for the 50° sweep model. In general, this theory may be taken as an upper limit in estimating center-line pressures on delta-wing planforms having sweep angles in the range covered in this investigation.

The proposed method of reference 10 is seen to yield fairly good agreement with the measured data for the sweep angles and angle-of-attack range of this investigation.

Surface Flows

The oil-flow technique has been successfully employed on various configurations to study surface flow behavior due to varying the angle of attack. (See refs. 12 to 14.) In figure 8, several selected photographs of surface flow patterns on the 75° sweep wing model at $M = 6.85$ are presented for the angle-of-attack range of this investigation. This model was fabricated to the same dimensions as the pressure model. At an angle of attack of 30°, the flow traces on the slab surface show that the flow moves along radial paths emanating from the wing apex toward the trailing edge of the wing. As angle of attack is increased, these flow traces become curved near the leading edges and also begin to exit over the leading edges. This curvature effect appears to be greatest at an angle of attack of about 75°. As angle of attack is increased further, the flow patterns become of a radial type originating from the stagnation regions which are discernible along the center line. At angles of attack of 80° and 85°, the shape of these high-pressure regions is not too well defined but the movement of these regions toward the wing trailing edge is indicated in the photographs as angle of attack is increased from 80° to 90°. This effect is also corroborated from the pressure coefficients listed in table I. Similar oil-flow studies on delta-wing planforms having blunt and sharp leading edges are presented in references 6, 15, and 16. At the highest angle of attack, a better-defined stagnation region is located approximately at the 77-percent-chord center-line station. For a flat, sharp-leading-edge delta wing, a theoretical location for the stagnation point is the 67-percent-chord station, which is confirmed from oil-flow traces obtained on a flat delta wing ($\Lambda = 75°$) at a free-stream Mach number of 9.6. (See ref. 15.) Further confirmation is also obtained from reference 17 in which location of the stagnation point is plotted against angle of attack. The results presented in reference 17 were obtained from center-line pressure measurements on a flat delta wing having 65° sweep at a free-stream Mach number of 5.97. For the blunted wing model of the present tests, it is realized that the nose section covers the first 16 percent of the center line. The theoretical stagnation-point location for the blunted wing should then be near the 72-percent-chord station. The resulting difference of 5-percent chord is considered fair agreement for this type of approximation.

CONCLUSIONS

Pressure distributions on four blunt delta wings having sweep angles of 50°, 70°, 75°, and 80° were obtained at a Mach number of 6.85 over an angle-of-attack

range from 30° to 90°. The following conclusions were obtained:

1. In general, the pressures on the windward slab surfaces are a function of angle of attack and are constant over the surfaces in the angle-of-attack range from 30° to 50°. As angle of attack is increased further, pressure gradients exist on both the windward slab and leading-edge surfaces due to bow-shock curvature.

2. Pressures on the windward leading edges decreased as distance from the wing apex increased, with significant pressure variations occurring in the angle-of-attack range from 50° to 90°.

3. Modified Newtonian predictions of the experimental pressures gave only fair results. On slab surfaces, theory underpredicted at angles of attack up to 60° but gave better agreement at the higher angles. On windward leading edges, theory overpredicted at angles of attack from 60° to 90° but gave better agreement at the lower angles.

4. The most significant effect of leading-edge sweep angle - that is, increase of pressures over the wing as sweep angle is decreased - is generally confined to angles of attack less than 60°.

5. The effect of angle of attack is best characterized by the fact that over 90 percent of the maximum pressure rise is attained at an angle of attack of 70°.

6. For the angle-of-attack range and sweep angles of these tests, the measured pressure coefficients on the model center line are bracketed by the five-term hypersonic approximation and modified Newtonian theory. The proposed method of NASA Technical Memorandum X-757 shows fairly good agreement with the measured data.

Langley Research Center,
National Aeronautics and Space Administration,
Langley Station, Hampton, Va., April 9, 1963.

REFERENCES

1. Staff of Langley Flight Research Division (Compiled by Donald C. Cheatham): A Concept of a Manned Satellite Reentry Which Is Completed With a Glide Landing. NASA TM X-226, 1959.

2. Ladson, Charles L., and Johnston, Patrick J.: Aerodynamic Characteristics of Two Winged Reentry Vehicles at Supersonic and Hypersonic Speeds. NASA TM X-346, 1961.

3. Reed, James D., and Shaw, David S.: Static Stability and Control Characteristics of a Proposed Winged Reentry Vehicle at Mach Numbers of 1.50, 2.96, and 4.63. NASA TM X-676, 1962.

4. McLellan, Charles H., Williams, Thomas W., and Bertram, Mitchel H.: Investigation of a Two-Step Nozzle in the Langley 11-Inch Hypersonic Tunnel. NACA TN 2171, 1950.

5. Bertram, Mitchel H.: Exploratory Investigation of Boundary-Layer Transition on a Hollow Cylinder at a Mach Number of 6.9. NACA Rep. 1313, 1957. (Supersedes NACA TN 3546.)

6. Bertram, Mitchel H., and Henderson, Arthur, Jr.: Recent Hypersonic Studies of Wings and Bodies. ARS Jour., vol. 31, no. 8, Aug. 1961, pp. 1129-1139.

7. Rainey, Robert W.: Working Charts for Rapid Prediction of Force and Pressure Coefficients on Arbitrary Bodies of Revolution by Use of Newtonian Concepts. NASA TN D-176, 1959.

8. Lees, Lester: Hypersonic Flow. Fifth International Aeronautical Conference (Los Angeles, Calif., June 20-23, 1955), Inst. Aero. Sci., Inc., 1955, pp. 241-276.

9. Mueller, James N. (With appendix by Eugene S. Love): Pressure Distributions on Blunt Delta Wings at a Mach Number of 2.91 and Angles of Attack up to to 90°. NASA TM X-623, 1962.

10. Fetterman, David E.: A Method for Predicting the Normal-Force Characteristics of Delta Wings at Angles of Attack of 0° to 90°. NASA TM X-757, 1963.

11. Penland, Jim A.: Aerodynamic Characteristics of a Circular Cylinder at Mach Number 6.86 and Angles of Attack up to 90°. NACA TN 3861, 1957. (Supersedes NACA RM L54A14.)

12. Bertram, Mitchel H., Feller, William V., and Dunavant, James C.: Flow Fields, Pressure Distributions, and Heat Transfer for Delta Wings at Hypersonic Speeds. NASA TM X-316, 1960.

13. Coe, Frank S., III, and Feller, William V.: Experimental Investigation of the Pressures, Heat Transfer, and Surface Flow Patterns Around a Blunt Half-Cone Lifting Reentry Body at a Mach Number of 9.6. NASA TM X-589, 1961.

14. Everhart, Philip E., and Bernot, Peter T.: Measurements of the Surface Flows, Heat Transfer, Pressure Distribution, and Longitudinal Stability of a Mercury Capsule Model at Mach Numbers of 6.9 and 9.6. NASA TM X-458, 1961.

15. Dunavant, James C.: Investigation of Heat Transfer and Pressures on Highly Swept Flat and Dihedraled Delta Wings at Mach Numbers of 6.8 and 9.6 and Angles of Attack to 90°. NASA TM X-688, 1962.

16. Bertram, Mitchel H., and Everhart, Philip E.: An Experimental Study of the Pressure and Heat-Transfer Distribution on a 70° Sweep Slab Delta Wing in Hypersonic Flow. NASA TR R-153, 1963.

17. Goldberg, Theodore J., and Hondros, James G.: Pressure Distributions on a Flat-Plate Delta Wing Swept 65° at a Mach Number of 5.97 at Angles of Attack From 65° to 115° and Angles of Roll From 0° to 25° at a 90° Angle of Attack. NASA TM X-702, 1962.

TABLE I.- ORIFICE LOCATIONS AND TABULATION OF MEASURED PRESSURE COEFFICIENTS

(a) 50° SWEEP ANGLE MODEL

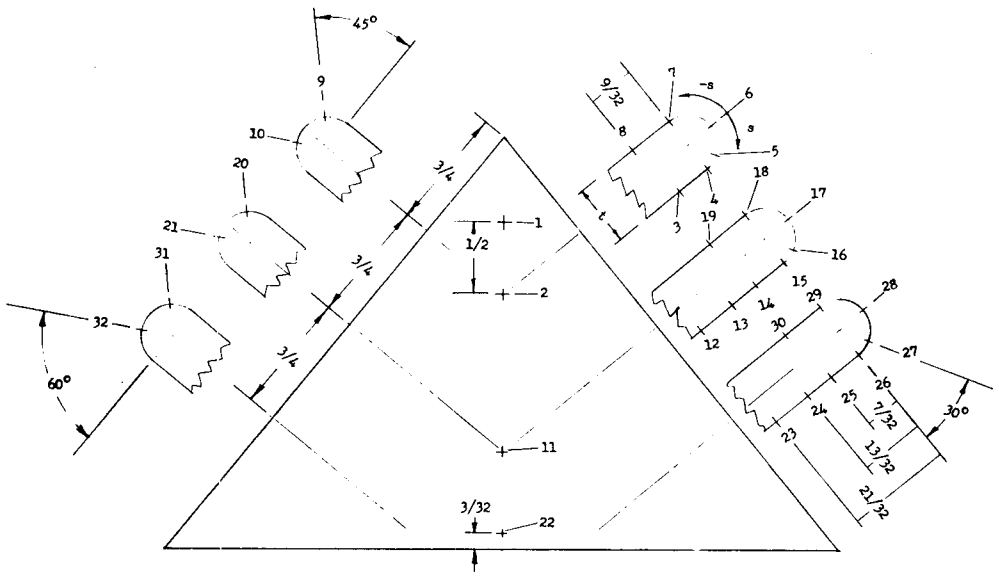

Windward orifice nos.: 1-6, 10-17, 21-28, 32

		Pressure coefficient, C_p											
s/t	Orifice No.	α = 35°	α = 40°	α = 45°	α = 50°	α = 55°	α = 60°	α = 65°	α = 70°	α = 75°	α = 80°	α = 85°	α = 90°
1.107	1	.721	.939	1.127	1.323	1.534	1.708	1.798	1.833	1.802	1.753	1.711	1.632
2.036	2	.731	.958	1.188	1.361	1.534	1.665	1.745	1.810	1.817	1.803	1.806	1.786
1.369	3	.732	1.035	1.150	1.358	1.550	1.688	1.753	1.805	1.794	1.780	1.757	1.732
0.785	4	.738	1.034	1.228	1.416	1.590	1.673	1.695	1.698	1.633	1.573	1.525	1.443
.524	5	1.062	1.231	1.354	1.443	1.493	1.460	1.402	1.317	1.196	1.067	.977	.846
0.000	6	-	-	-	-	-	-	-	-	.179	-	-	-
- .785	7	-.002	-.006	-.007	-.008	-.004	-.001	.002	.002	.004	.000	.002	.002
-1.535	8	-.003	-.005	-.006	-.007	-.004	-.004	.000	.001	.001	-.004	.000	.000
- .393	9	.079	.058	.043	.030	.018	.016	.004	-.003	-.006	-.006	-.001	.001
.262	10	.990	1.010	1.003	.979	.931	.844	.718	.594	.496	.399	.332	.257
3.701	11	.750	.961	1.134	1.321	1.476	1.532	1.588	1.653	1.685	1.730	1.796	1.837
2.536	12	.727	.949	1.136	1.313	1.492	1.581	1.638	1.702	1.725	1.757	1.811	1.837
1.869	13	.747	.967	1.156	1.349	1.519	1.565	1.623	1.687	1.691	1.703	1.748	1.772
1.369	14	.773	1.001	1.010	1.385	1.534	1.636	1.684	1.727	1.702	1.719	1.760	1.760
.785	15	.882	1.100	1.276	1.436	1.527	1.565	1.574	1.572	1.517	1.489	1.491	1.466
.524	16	1.062	1.215	1.324	1.410	1.408	1.351	1.303	1.236	1.159	1.067	1.014	.929
0.000	17	.526	.491	.432	.370	.356	.231	.188	.144	.109	.075	.054	.035
- .785	18	-.003	-.004	-.005	-.005	-.002	.002	.005	.005	.004	.001	.003	.004
-1.535	19	-.004	-.006	-.006	-.005	-.004	.003	.002	.002	.002	-.003	.000	.000
- .393	20	.062	.043	.031	.018	.007	-.000	-.004	-.005	-.002	-.002	.000	.000
.262	21	.996	1.015	1.013	.945	.870	.774	.710	.5722	.493	.415	.362	.300
4.407	22	.710	.910	1.087	1.239	1.273	1.274	1.318	1.380	1.409	1.473	1.568	1.652
2.536	23	.662	.873	1.065	1.256	1.347	1.427	1.463	1.537	1.564	1.635	1.717	1.806
1.869	24	.748	.958	1.151	1.352	1.475	1.520	1.585	1.649	1.656	1.703	1.756	1.821
1.369	25	.764	.976	1.170	1.367	1.495	1.550	1.611	1.644	1.679	1.696	1.731	1.752
.785	26	.884	1.094	1.270	1.413	1.500	1.516	1.532	1.549	1.533	1.516	1.538	1.525
.524	27	1.007	1.180	1.293	1.372	1.388	1.343	1.300	1.284	1.236	1.168	1.145	1.087
0.000	28	.568	.507	.439	.366	.355	.235	.191	.152	-	.090	.072	.054
- .785	29	-.013	-.012	-.010	-.008	-.005	-.003	.000	.001	.001	-.001	-.000	-.002
-1.535	30	-.004	-.006	-.007	-.005	-.003	-.005	.023	-	-	-	-	-
- .393	31	-	-	-	-	-	-	-	-	-	-	-	-
.262	32	.990	.999	.967	.894	.793	.702	.648	.537	.476	.421	.370	.323

TABLE I.- CONTINUED

(b) 70° SWEEP ANGLE MODEL

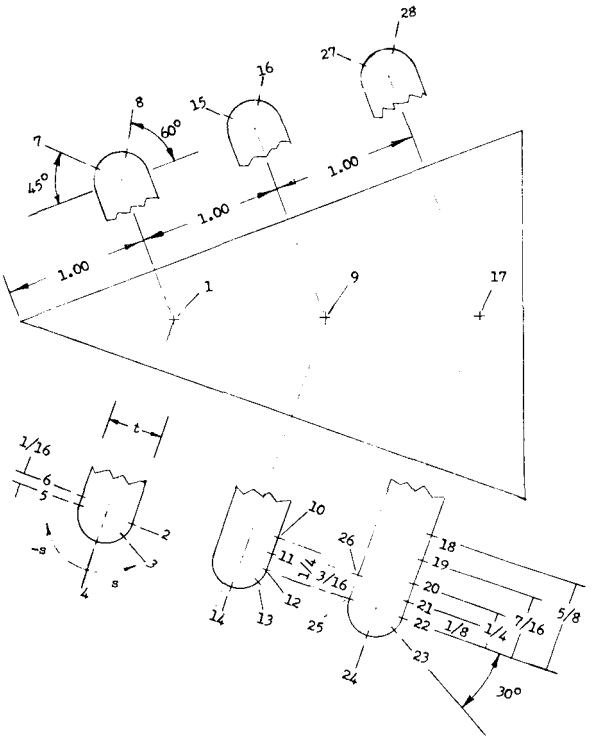

Windward orifice nos.: 1-4, 8-14, 16-24, 28

s/t	Orifice No.	Pressure coefficient, C_p												
		α = 30°	α = 35°	α = 40°	α = 45°	α = 50°	α = 55°	α = 60°	α = 65°	α = 70°	α = 75°	α = 80°	α = 85°	α = 90°
1.257	1	.642	.776	.950	1.116	1.285	1.451	1.552	1.682	1.758	1.796	1.799	1.772	1.712
.785	2	.717	.706	.887	1.047	1.200	1.349	1.529	1.628	1.684	1.696	1.691	1.639	1.548
.524	3	.639	.765	.875	.974	1.060	1.130	1.220	1.241	1.233	1.198	1.125	1.049	.922
0.000	4	.118	.183	.178	.173	.168	.163	.172	.164	.150	.129	.110	.090	.069
-.785	5	.001	-.001	-.007	-.009	-.009	-.009	-.007	-.004	-.003	-.004	-.003	-.003	-.004
-.962	6	.001	-.003	-.009	-.011	-.010	-.009	-.007	-.005	-.005	-.005	-.004	-.004	-.005
-.393	7	.001	-.004	-.007	-.007	-.009	-.009	-.009	-.008	-.005	-.004	-.002	-.003	-.003
.262	8	.456	.499	.535	.562	.582	.588	.567	.560	.531	.488	.441	.386	.325
2.227	9	.591	.745	.912	1.068	1.230	1.379	1.502	1.616	1.697	1.731	1.770	1.773	1.757
1.451	10	.581	.752	.919	1.089	1.245	1.377	1.498	1.616	1.685	1.731	1.759	1.739	1.720
1.118	11	.610	.771	.931	1.084	1.234	1.371	1.490	1.582	1.647	1.673	1.699	1.739	1.661
.785	12	.623	.778	.941	1.078	1.194	1.297	1.378	1.457	1.483	–	–	–	1.451
.524	13	.629	.746	.849	.922	.974	1.020	1.110	1.093	1.078	1.044	1.003	.943	.892
0.000	14	–	.209	.200	.190	.186	.173	.174	.159	.142	.122	.106	.090	.069
-.393	15	.001	-.006	-.009	-.010	-.012	-.009	.000	-.000	-.002	.002	.001	.002	-.000
.262	16	.421	.458	.483	.498	.505	.494	.455	.430	.427	.364	.334	.298	.286
3.198	17	.495	.681	.872	1.038	1.222	1.389	1.418	1.454	1.507	1.563	1.625	1.673	1.673
2.451	18	.526	.688	.863	1.034	1.217	1.387	1.455	1.506	1.558	1.636	1.706	1.747	1.785
1.951	19	.529	.691	.859	1.031	1.203	1.389	1.447	1.513	1.580	1.636	1.691	1.724	1.770
1.451	20	.545	.705	.872	1.032	1.203	1.365	1.477	1.535	1.595	1.629	1.714	1.739	1.727
1.118	21	.572	.737	.893	1.044	1.201	1.354	1.447	1.513	1.558	1.592	1.655	1.665	1.669
.785	22	.607	.764	.912	1.040	1.162	1.277	1.337	1.381	1.418	1.468	1.507	1.481	1.494
.524	23	.616	.703	.790	.849	.895	.922	.973	.967	.935	.923	.909	.871	.826
0.000	24	–	.181	.178	.166	.153	.138	.136	.118	.103	.091	.080	.069	.059
-.785	25	-.018	-.009	-.008	-.008	-.007	-.005	-.004	-.002	.000	.000	.000	.000	.000
-1.285	26	-.016	-.013	-.012	-.013	-.010	-.009	-.007	-.005	-.003	-.003	-.002	-.001	-.002
-.393	27	-.006	-.008	-.011	-.013	-.014	-.015	-.011	-.007	-.002	-.001	-.001	-.000	-.002
.262	28	.416	.449	.466	.471	.466	.451	.402	.371	.347	.333	.312	.291	.264

TABLE I.- CONTINUED

(c) 75° SWEEP ANGLE MODEL

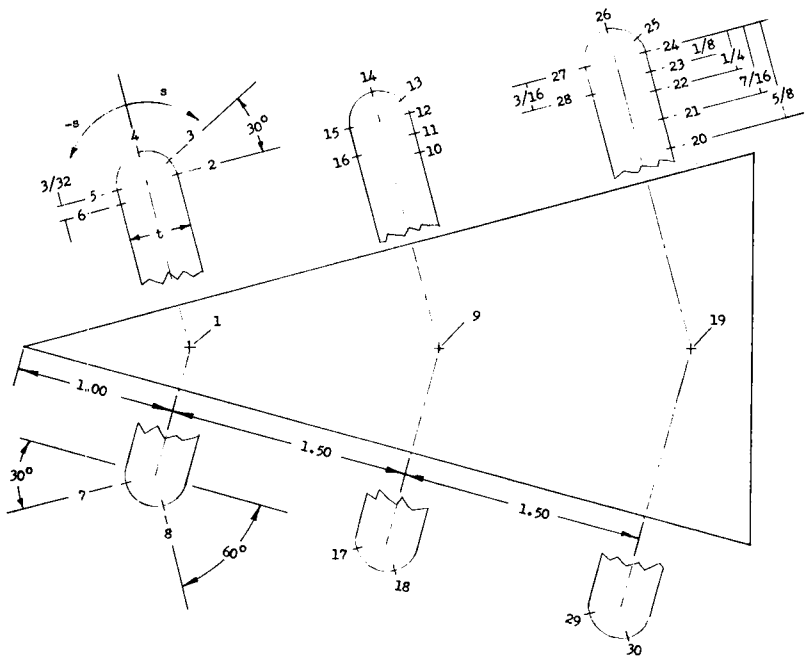

Windward orifice nos.: 1-4, 8-14, 18-26, 30

s/t	Orifice No.	Pressure coefficient, C_p												
		α = 30°	α = 35°	α = 40°	α = 45°	α = 50°	α = 55°	α = 60°	α = 65°	α = 70°	α = 75°	α = 80°	α = 85°	α = 90°
1.035	1	.5167	.669	.837	1.008	1.201	1.355	1.489	1.675	1.761	1.835	1.850	1.825	1.721
.785	2	.540	.698	.866	1.032	1.210	1.351	1.498	1.634	1.712	1.781	1.795	1.752	1.667
.524	3	.566	.693	.824	.930	1.061	1.143	1.188	1.279	1.308	1.313	1.285	1.222	1.124
0.000	4	.139	.142	.144	.145	.151	.152	.143	.146	.144	.137	.122	.109	.090
- .785	5	.005	-.001	-.006	-.010	-.010	-.009	-.002	-.000	-.003	-.002	-.004	-.003	-.004
-1.035	6	.008	-.002	-.003	-.007	-.008	-.007	-.001	.002	-.001	-.000	-.002	-.005	-.002
- .524	7	-.000	-.006	-.010	-.010	-.011	-.012	-.007	-.008	-.009	-.009	-.009	-.005	-.006
.262	8	.309	.352	.392	.427	.468	.473	.529	.543	.537	.516	.475	.435	.381
2.073	9	.536	.693	.892	1.032	1.215	1.363	1.488	1.622	1.709	1.772	1.815	1.812	1.787
1.451	10	.542	.696	.859	1.026	1.210	1.360	1.468	1.615	1.690	1.743	1.778	1.789	1.756
1.118	11	.547	.699	.863	1.024	1.205	1.348	1.449	1.567	1.647	1.701	1.726	1.728	1.690
.785	12	.572	.724	.878	1.024	1.191	1.302	1.371	1.487	1.517	1.567	1.574	1.577	1.532
.524	13	.539	.648	.745	.836	.914	.975	.989	1.036	1.035	1.028	1.001	.972	.908
0.000	14	.142	.144	.144	.143	.144	.138	.124	.112	.102	.089	.076	.065	.052
- .785	15	.009	.003	-.002	-.004	-.005	-.004	.005	.006	.003	.002	-.002	.001	-.001
-1.285	16	.010	.007	.001	-.001	-.004	-.002	.006	.006	.004	.003	-.002	.001	-.002
- .524	17	.008	-.003	-.009	-.011	-.012	-.013	.000	.003	.007	.003	.002	.002	.000
.262	18	.280	.309	.325	.346	.359	.357	.362	.339	.329	.307	.281	.256	.227
3.145	19	.528	.685	.859	1.029	1.229	1.398	1.534	1.590	1.638	1.669	1.753	1.784	1.823
2.451	20	.542	.698	.870	1.041	1.234	1.406	1.475	1.528	1.575	1.632	1.701	1.757	1.765
1.951	21	.538	.692	.862	1.031	1.234	1.388	1.557	1.534	1.602	1.636	1.710	1.735	1.768
1.451	22	-	-	-	-	-	-	1.498	-	-	-	-	-	1.755
1.118	23	.539	.692	.854	1.015	1.202	1.342	1.426	1.487	1.536	1.587	1.648	1.680	1.685
.785	24	.549	.690	.835	.966	1.112	1.227	1.295	1.350	1.381	1.414	1.460	1.491	1.479
.524	25	.517	.612	.705	.797	.870	.933	.935	.992	.977	.988	1.006	1.013	.997
0.000	26	.124	.121	.114	.137	.102	.093	.073	.064	.059	.049	.044	.048	.037
- .785	27	-.009	.001	-.002	-.005	-.008	-.006	-.007	-.004	-.005	-.004	-.005	-.002	-.002
-1.285	28	-.010	-.002	-.004	-.008	-.010	-.008	-.000	-.002	-.001	-.002	-.003	-.000	-.001
- .524	29	-.001	-.003	-.006	-.008	-.008	-.012	-.008	-.011	-.012	-.009	-.008	-.007	-.005
.262	30	.229	.249	.264	.277	.283	.279	.284	.260	.246	.236	.227	.215	.203

TABLE I.- CONCLUDED

(d) 80° SWEEP ANGLE MODEL

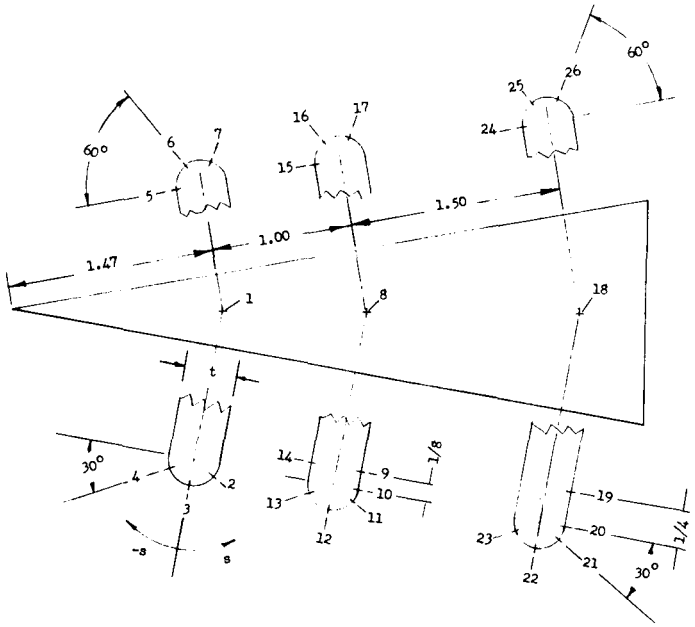

Windward orifice nos.: 1-3, 7-12, 17-22, 26

s/t	Orifice No.	Pressure coefficient, C_p												
		α = 30°	α = 35°	α = 40°	α = 45°	α = 50°	α = 55°	α = 60°	α = 65°	α = 70°	α = 75°	α = 80°	α = 85°	α = 90°
.977	1	.525	.672	.849	1.021	1.195	1.353	1.479	1.607	1.714	1.780	1.828	1.816	1.785
.524	2	.502	.539	.693	.858	1.028	1.148	.705	.747	.791	.808	.823	.805	.775
.000	3	.079	.086	.092	.099	.106	.111	.114	.115	.116	.115	.111	.102	.096
-0.524	4	.006	-.004	-.006	-.006	-.005	-.003	-.003	.006	.008	.008	.008	.005	.004
-0.785	5	.004	-.005	-.007	-.007	-.006	-.004	-.004	.006	.008	.008	.005	.005	.003
-0.262	6	.004	-.007	-.009	-.007	-.005	-.005	-.005	-.000	.000	.000	-.002	-.003	-.003
0.262	7	.285	.340	.399	.456	.514	.563	.593	.625	.650	.660	.650	.621	.592
1.447	8	.531	.680	.856	1.026	1.202	1.366	1.504	1.597	1.680	1.747	1.795	1.771	1.768
1.118	9	.532	.677	.847	1.017	1.194	1.349	1.482	1.586	1.669	1.725	1.776	1.760	1.746
.785	10	.531	.667	.829	.987	1.149	1.287	1.395	1.483	1.561	1.614	1.654	1.634	1.613
.524	11	.495	.610	.721	.837	.950	1.043	1.113	1.170	1.213	1.236	1.235	1.195	1.171
.000	12	.080	.086	.091	.097	.103	.106	.106	.104	.102	.099	.092	.085	.075
-0.524	13	.008	-.004	-.007	-.007	-.004	-.002	.000	.009	.009	.009	.009	.007	.006
-1.118	14	.010	-.002	-.005	-.004	-.001	.000	.002	.009	.011	.011	.011	.009	.008
-0.785	15	.010	-.002	-.003	-.004	-.002	.000	.002	.010	.012	.012	.012	.010	.009
-0.262	16	.006	-.006	-.007	-.006	-.004	-.004	-.002	.002	.003	.003	.003	.002	.003
0.262	17	.283	.333	.386	.437	.485	.523	.548	.566	.574	.574	.562	.529	.500
2.152	18	.504	.646	.818	.980	1.175	1.341	1.472	1.567	1.635	1.703	1.761	1.808	1.819
1.451	19	.610	.667	.811	.977	1.153	1.324	1.466	1.545	1.631	1.696	1.743	1.780	1.805
0.785	20	.506	.633	.781	.940	1.076	1.211	1.275	1.354	1.383	1.459	1.502	1.528	1.539
0.524	21	.442	.526	.622	.718	.805	.880	.929	.963	1.006	1.029	1.043	1.048	1.045
.000	22	.076	.080	.082	.087	.090	.090	.088	.085	.079	.076	.072	.064	.061
-0.524	23	-.014	-.015	-.014	-.012	-.009	-.008	-.006	-.005	-.001	.001	.003	.003	.005
-0.785	24	-.011	-.015	-.015	-.013	-.010	-.008	-.007	-.006	-.003	-.000	.001	.001	.00
-0.262	25	-.010	-.013	-.013	-.013	-.013	-.013	-.013	-.013	-.010	-.007	-.004	-.002	.0
0.262	26	.240	.277	.316	.353	.384	.409	.427	.439	.439	.439	.436	.424	

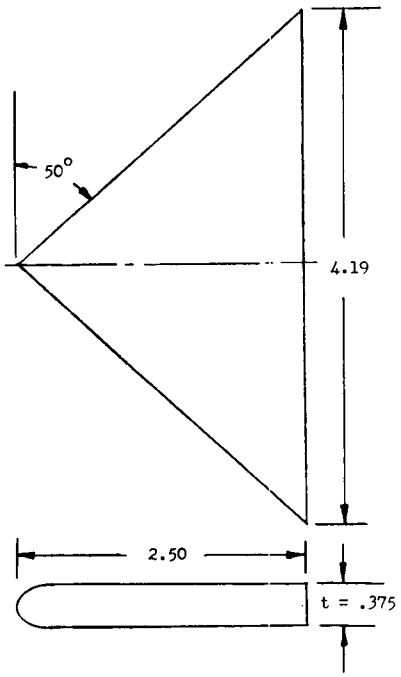

50° sweep delta wing

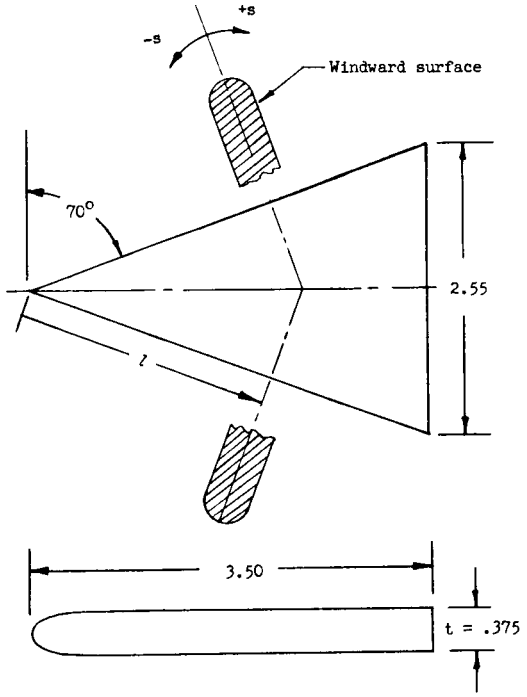

70° sweep delta wing

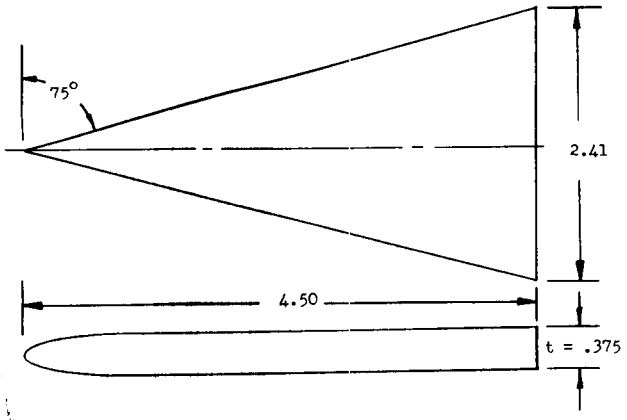

75° sweep delta wing

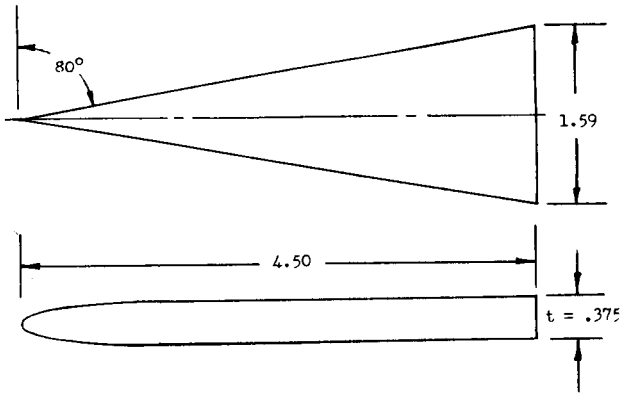

80° sweep delta wing

Figure 1.- Geometric details of test models. All linear dimensions are in inches.

Figure 2.- Typical test model with sting attached.

L-63-3101

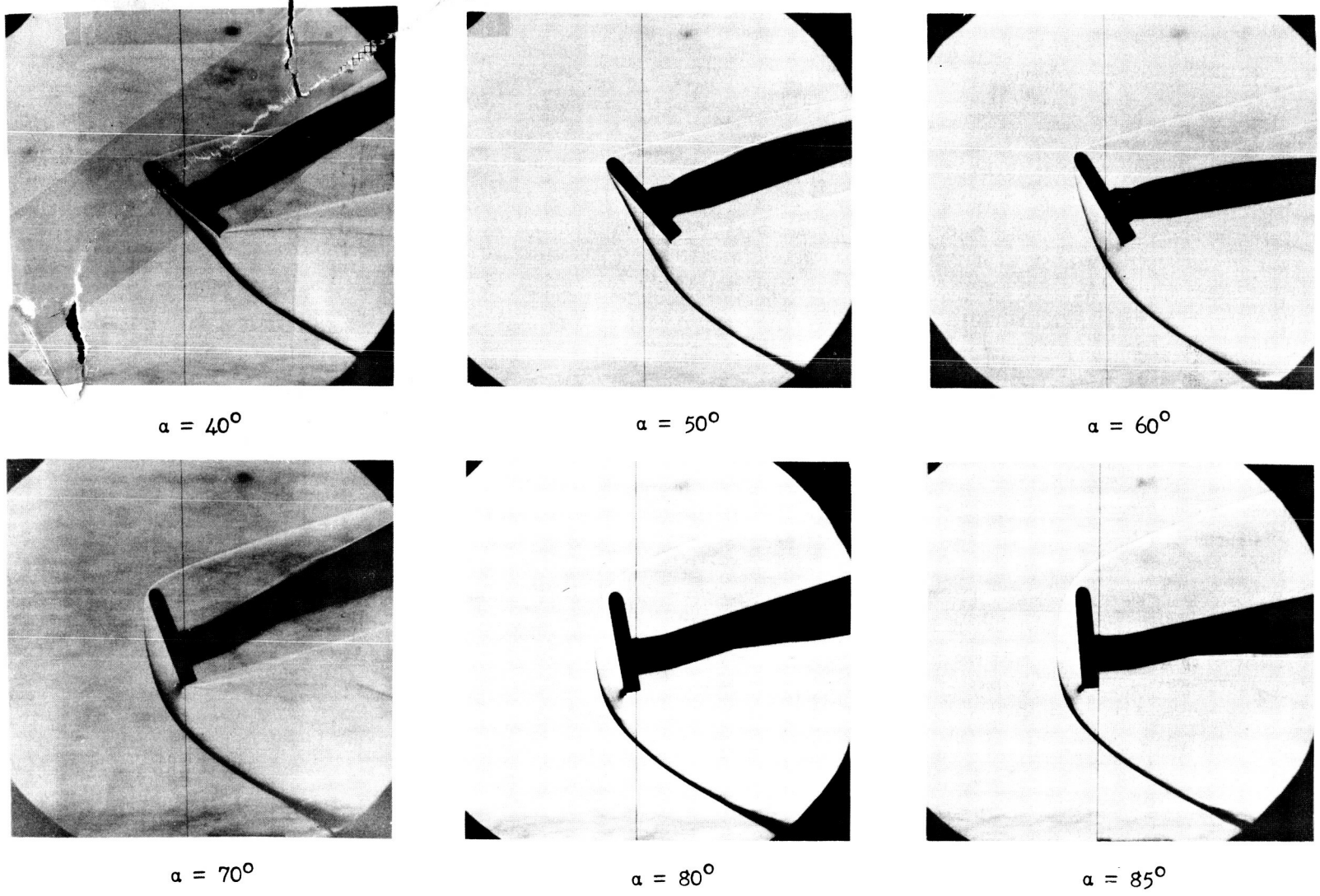

(a) 50° sweep delta wing.

L-63-3102

Figure 3.- Schlieren photographs of delta-wing models. (Photograph not available for $\alpha = 90°$.)

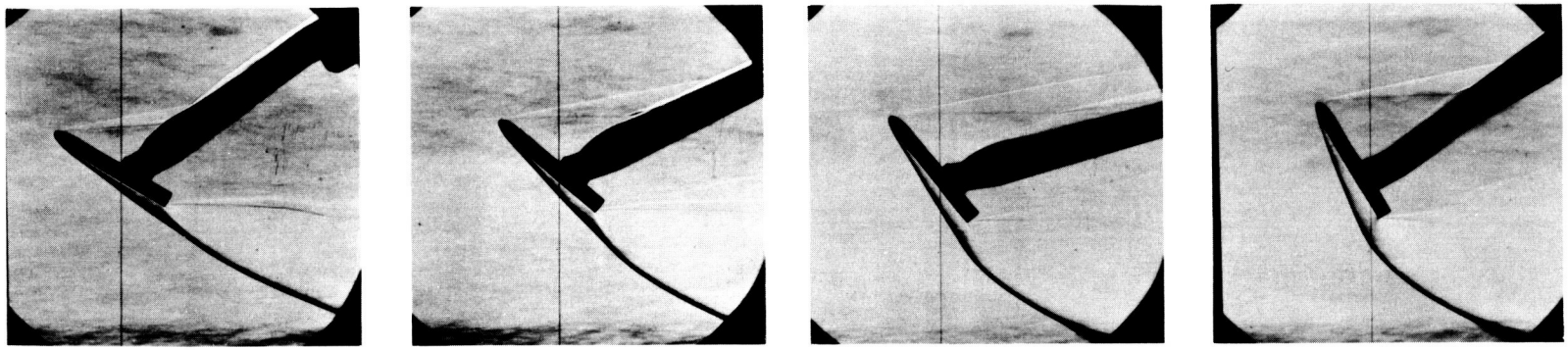

α = 30° α = 40° α = 50° α = 60°

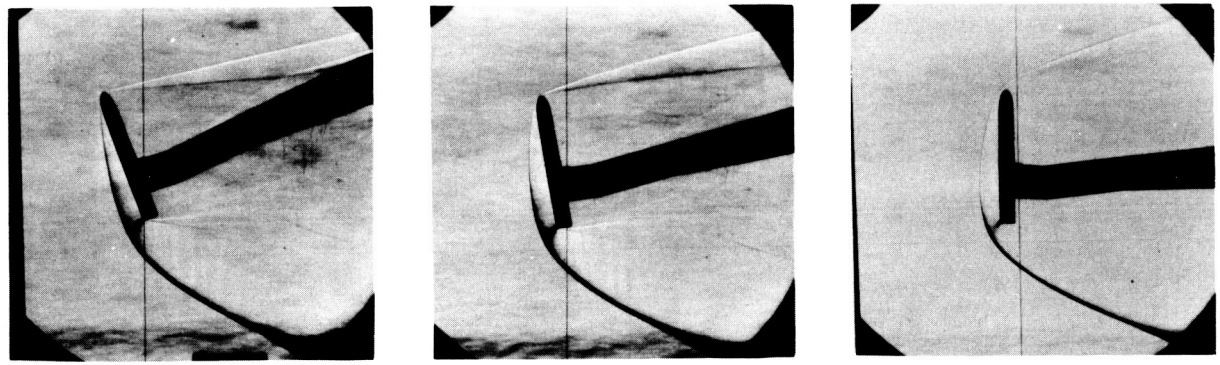

α = 70° α = 80° α = 90°

(b) 70° sweep delta wing.

L-63-3103

Figure 3.- Continued.

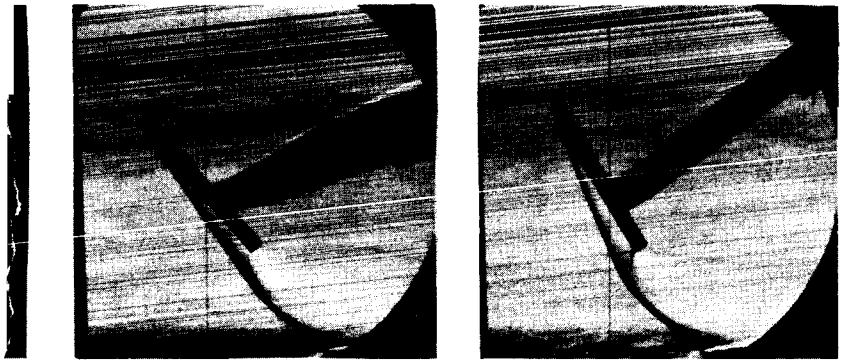

$\alpha = 50^{\circ}$ $\alpha = 60^{\circ}$

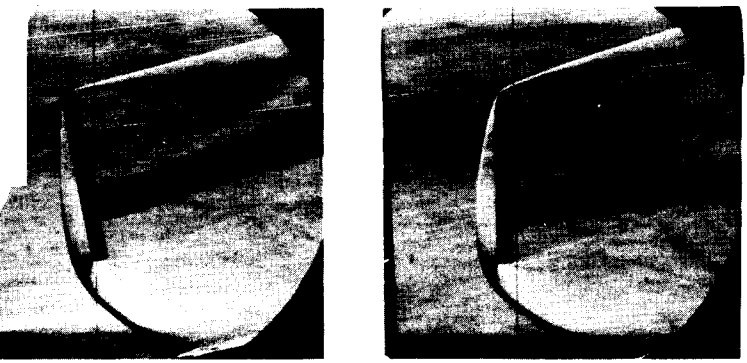

$\alpha = 80^{\circ}$ $\alpha = 90^{\circ}$

(c) 75° sweep delta wing. L-63-3104

Figure 3.- Continued.

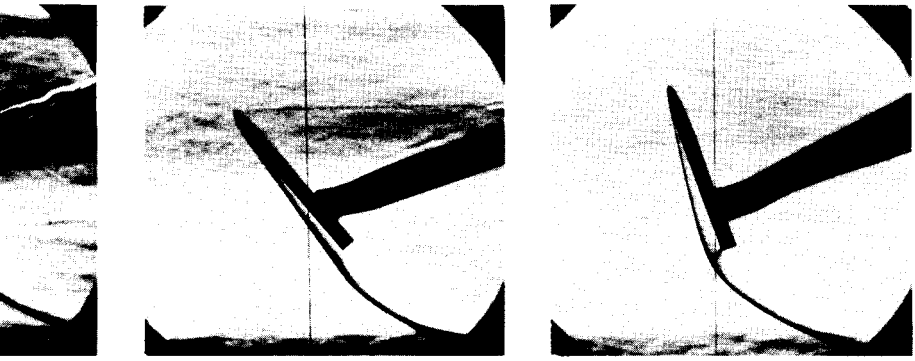

$\alpha = 50^{\circ}$ $\alpha = 60^{\circ}$

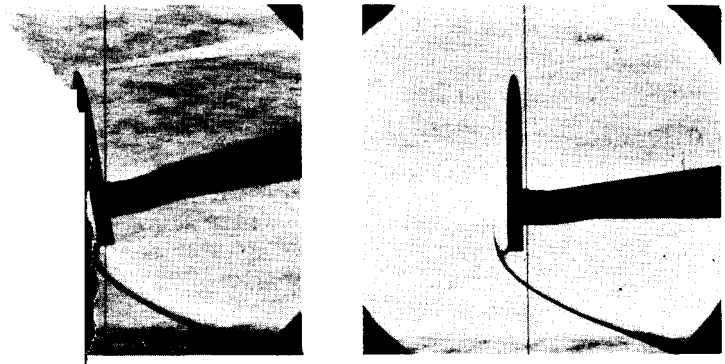

$\alpha = 80^{\circ}$ $\alpha = 90^{\circ}$

weep delta wing.

L-63-3105

- Concluded.

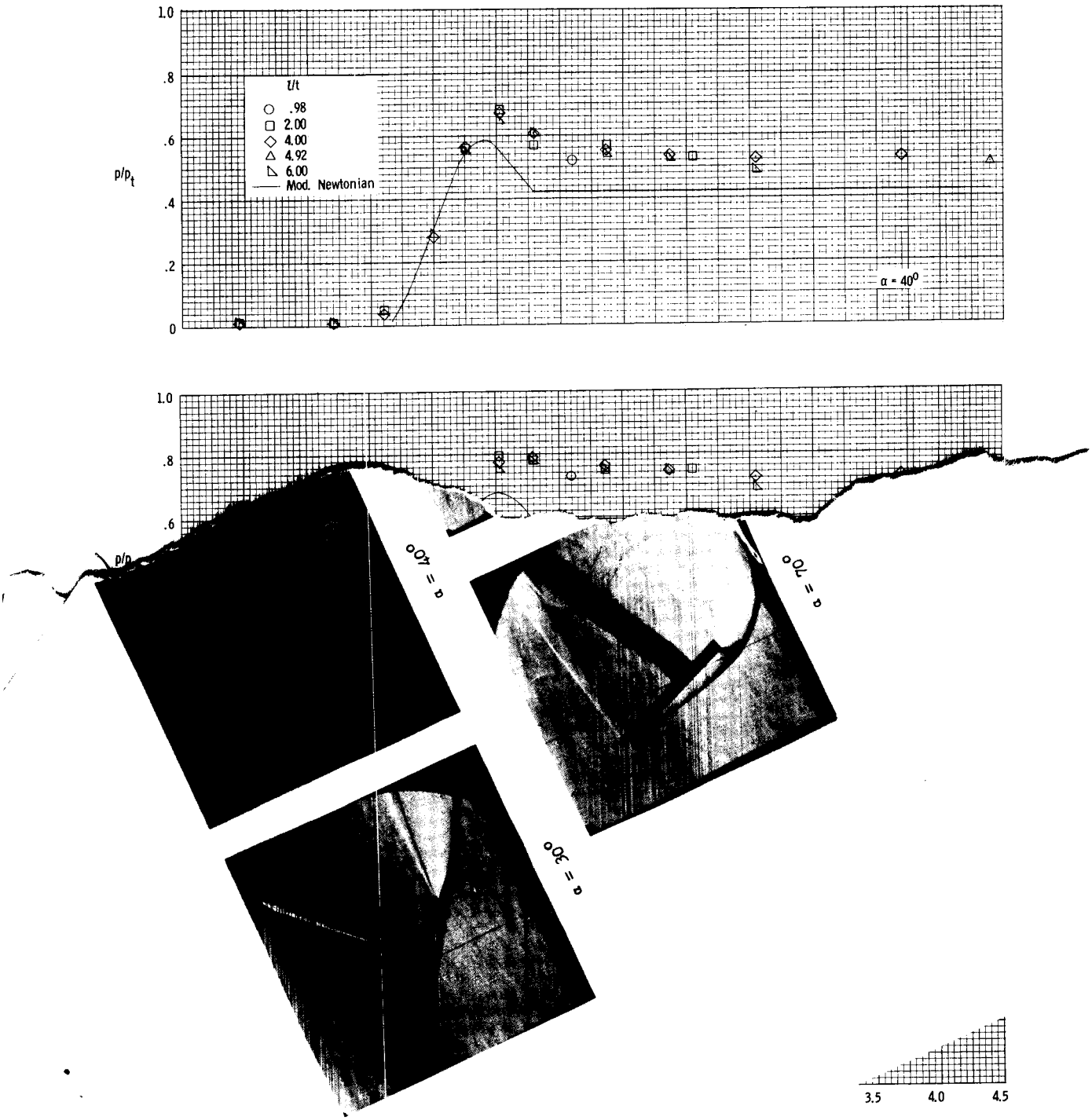

...e distributions - basic plots.

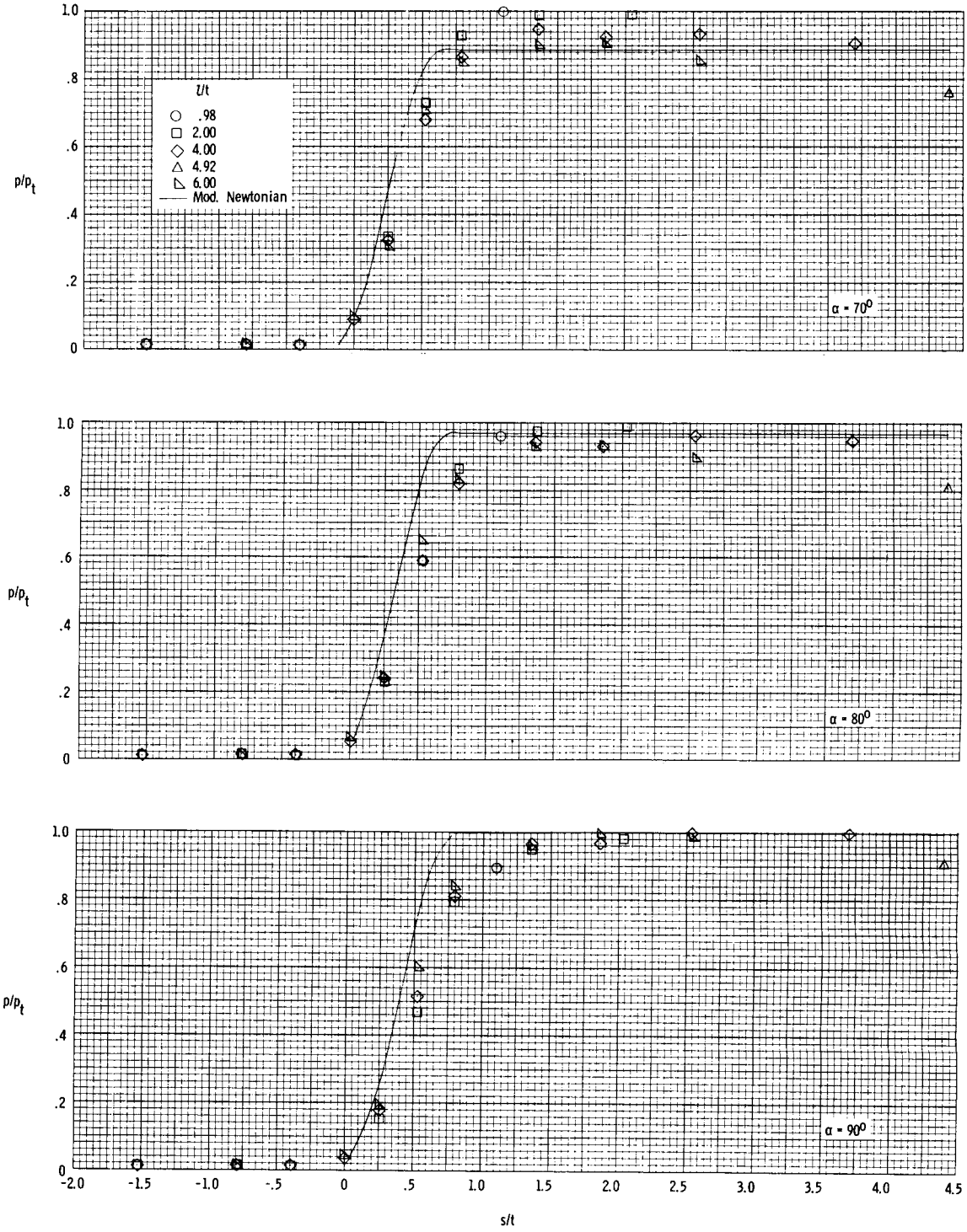

(a) $\Lambda = 50^{\circ}$. Concluded.

Figure 4.- Continued.

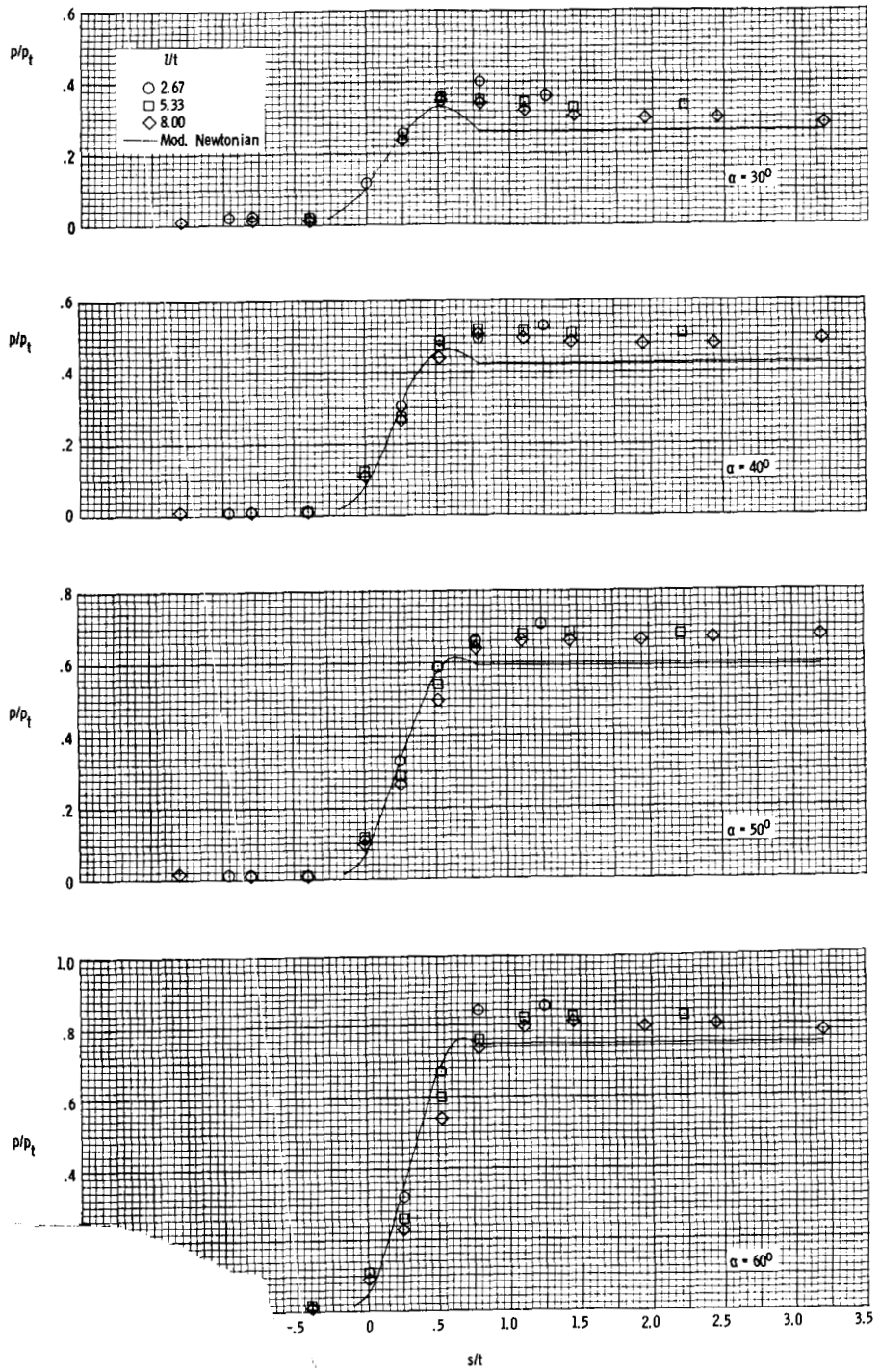

(b) $\Lambda = 70^{\circ}$.

Figure 4.- Continued.

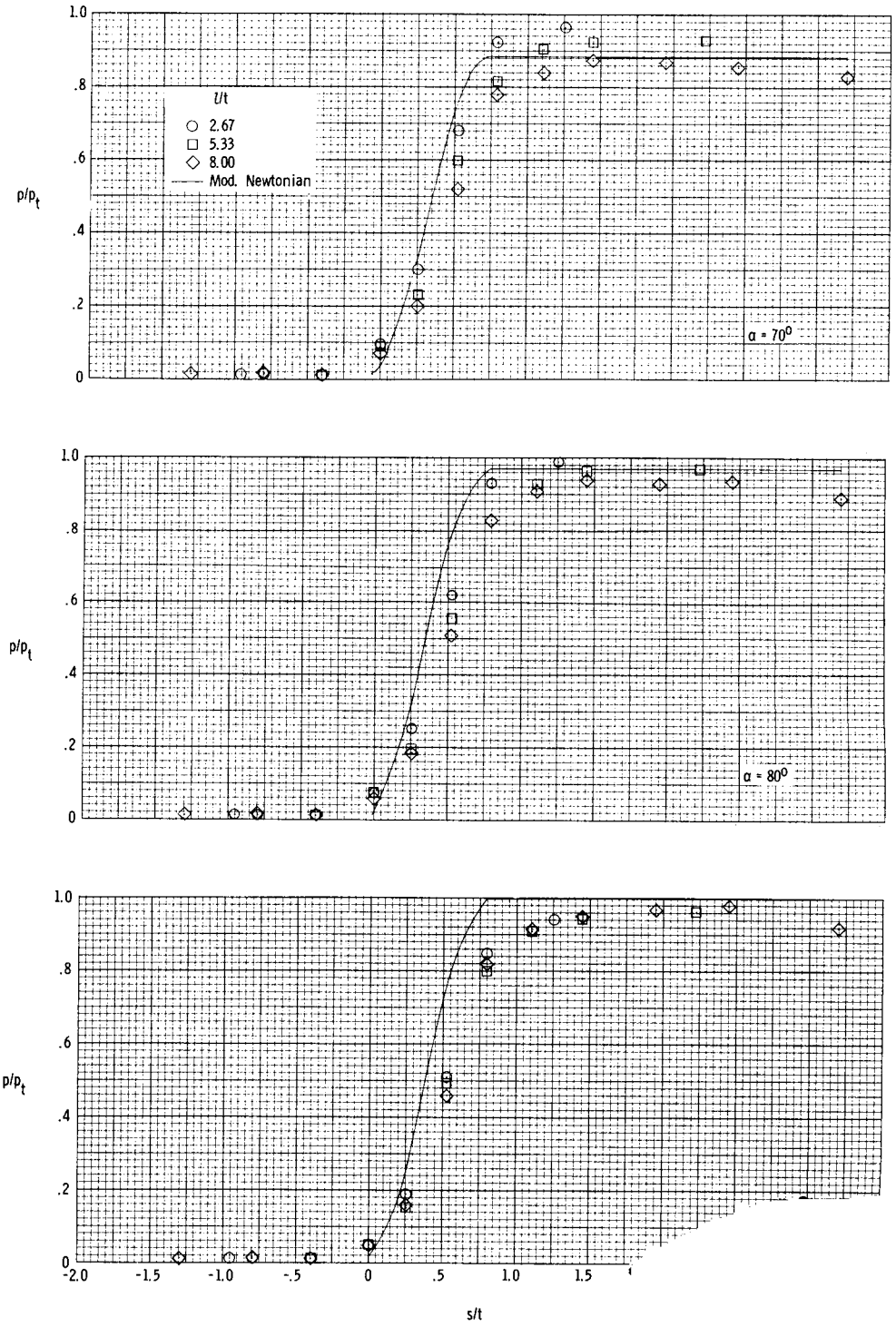

(b) $\Lambda = 70^{\circ}$. Conclud

Figure 4.- Continue

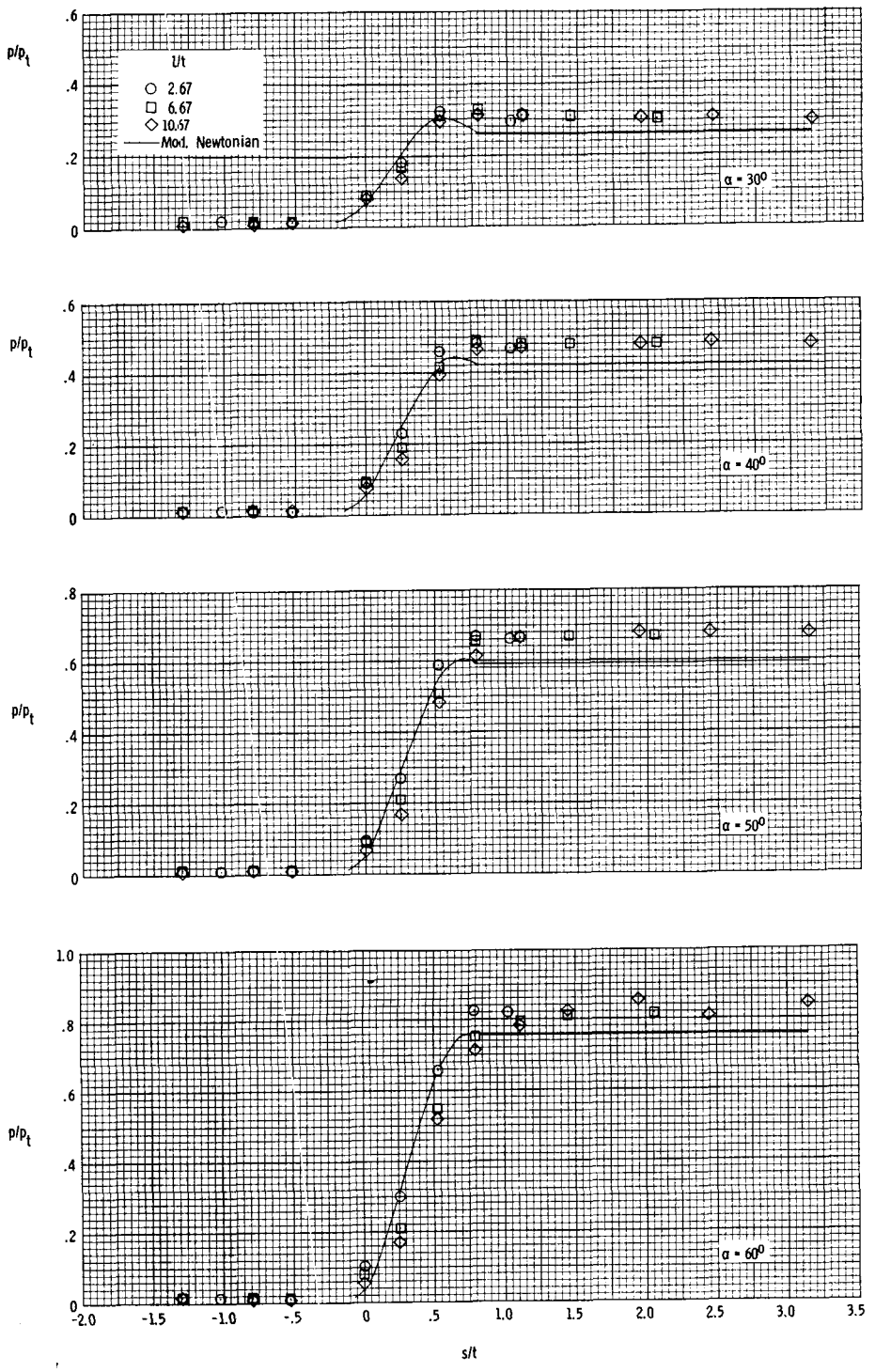

(c) $\Lambda = 75^{\circ}$.

Figure 4.- Continued.

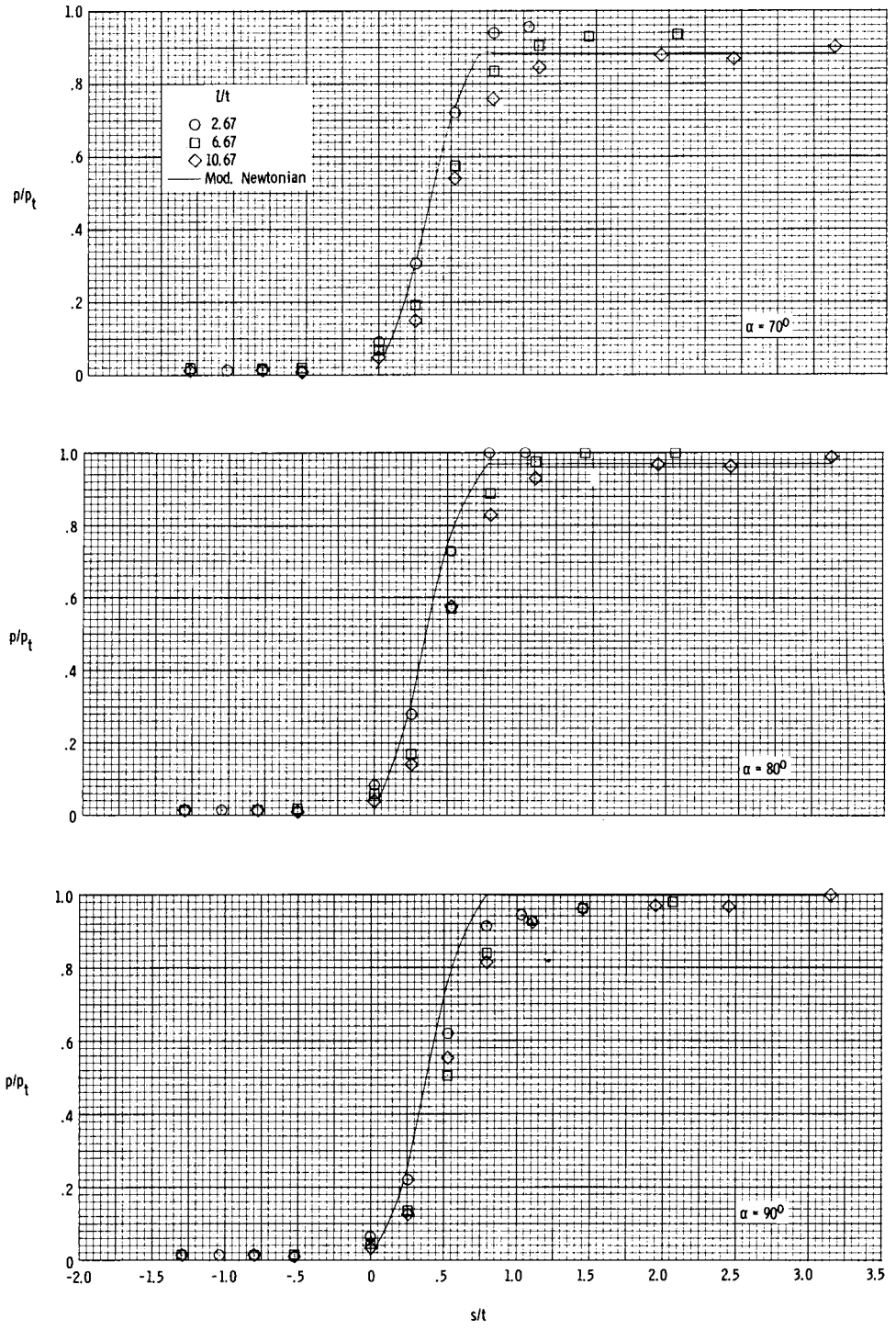

(c) $\Lambda = 75^{\circ}$. Concluded.

Figure 4.- Continued.

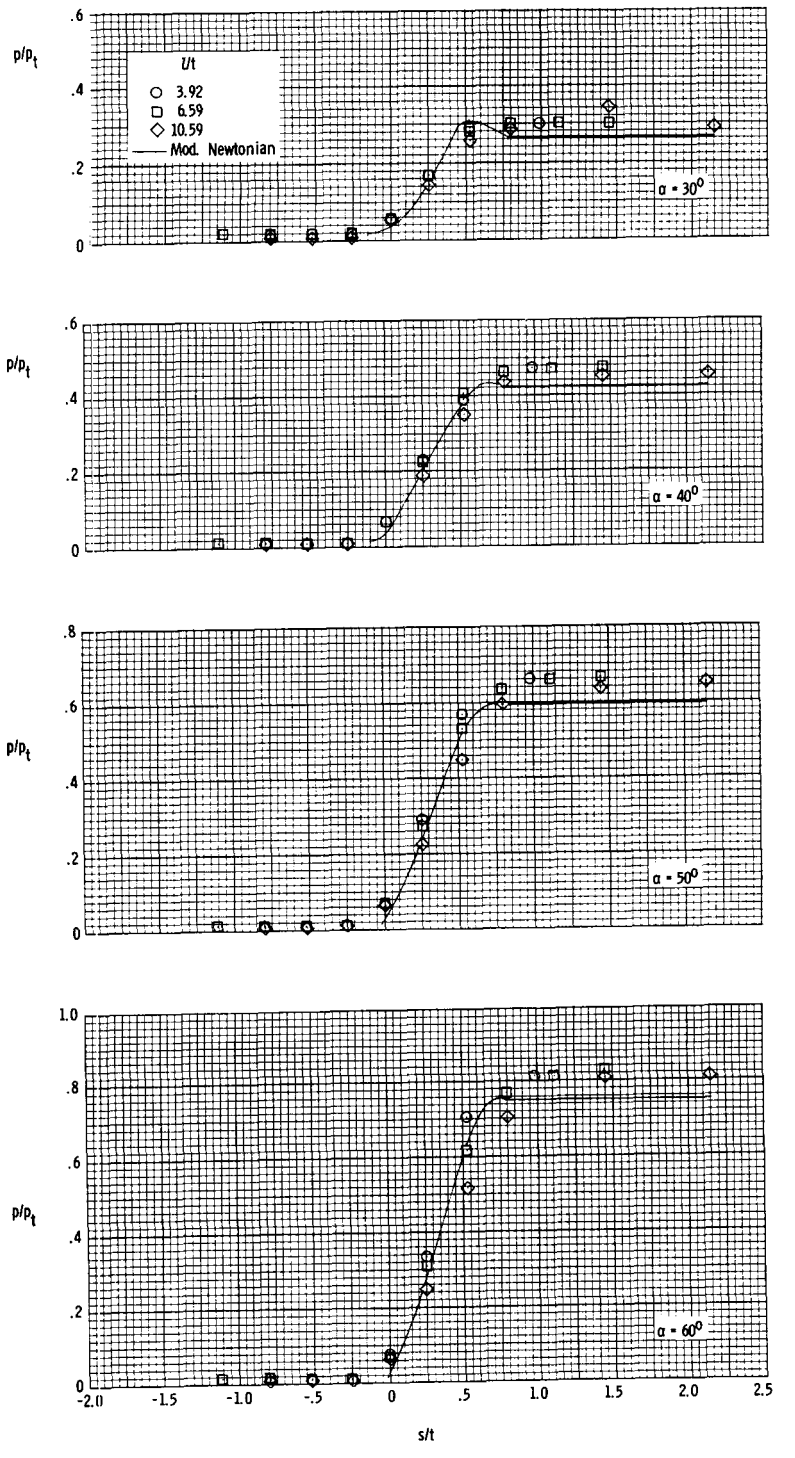

(d) $\Lambda = 80^{\circ}$.

Figure 4.- Continued.

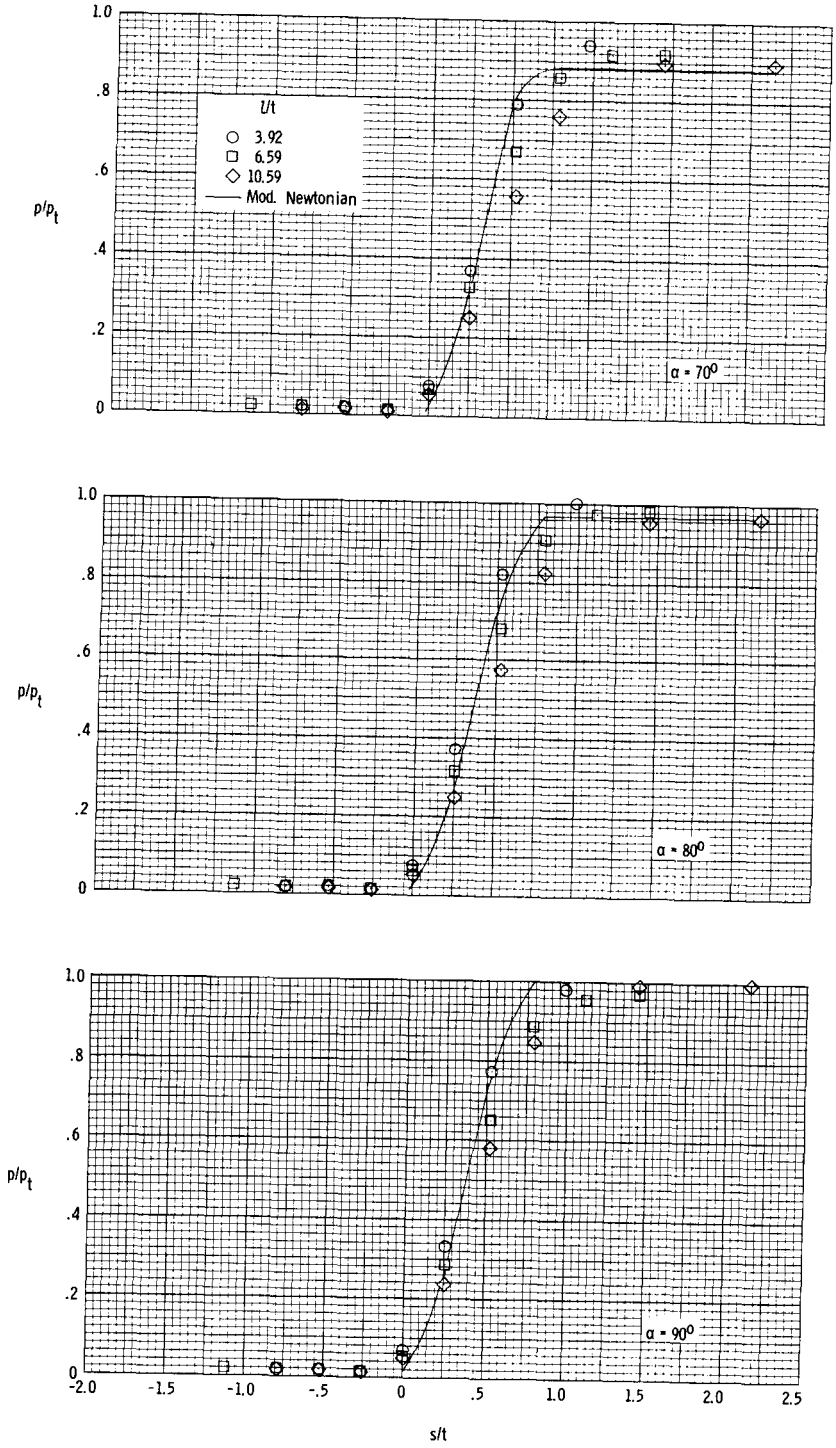

(d) $\Lambda = 80^{\circ}$. Concluded.

Figure 4.- Concluded.

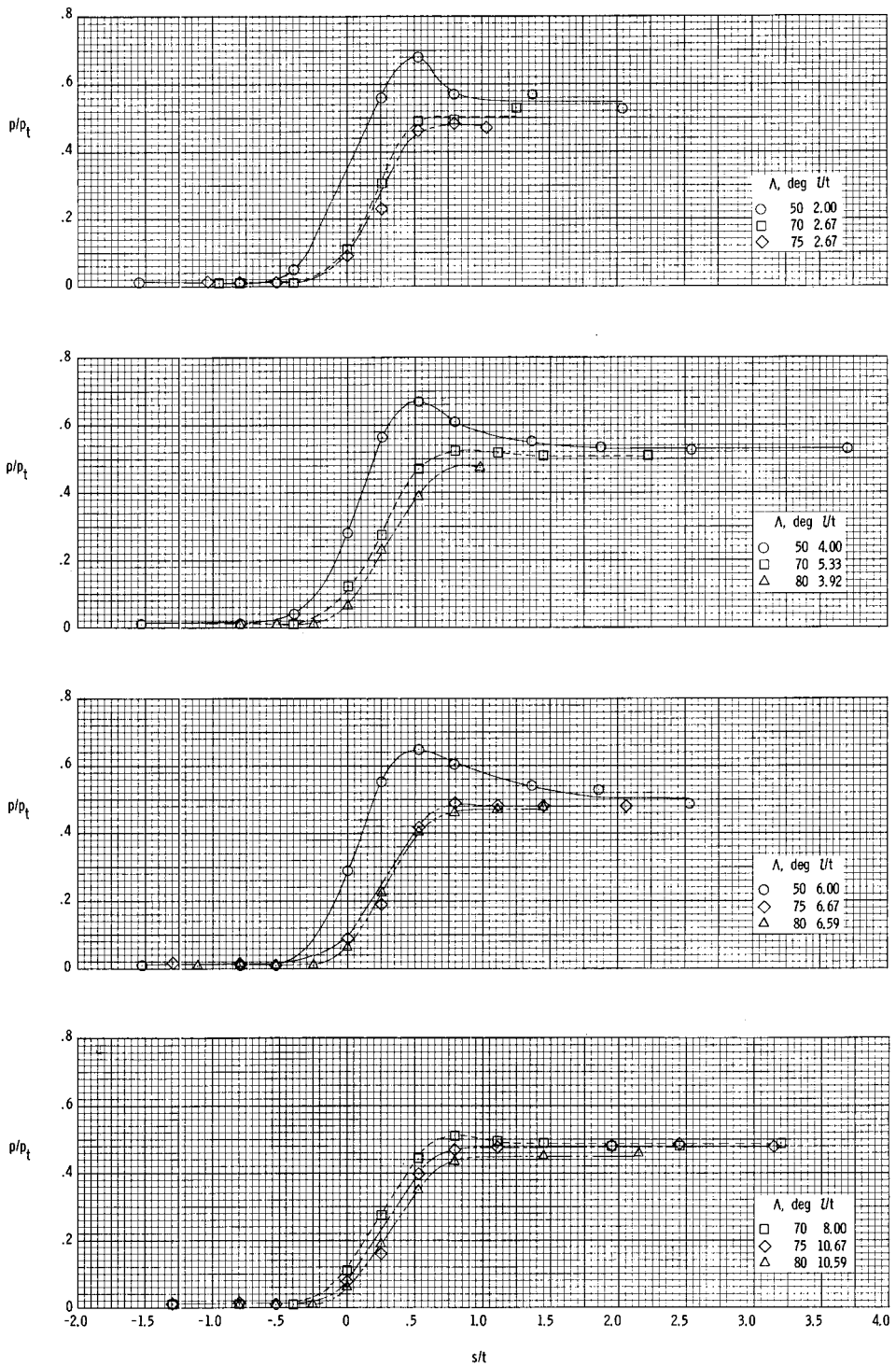

(a) $\alpha = 40^\circ$.

Figure 5.- Effect of wing sweep angle on pressure distributions.

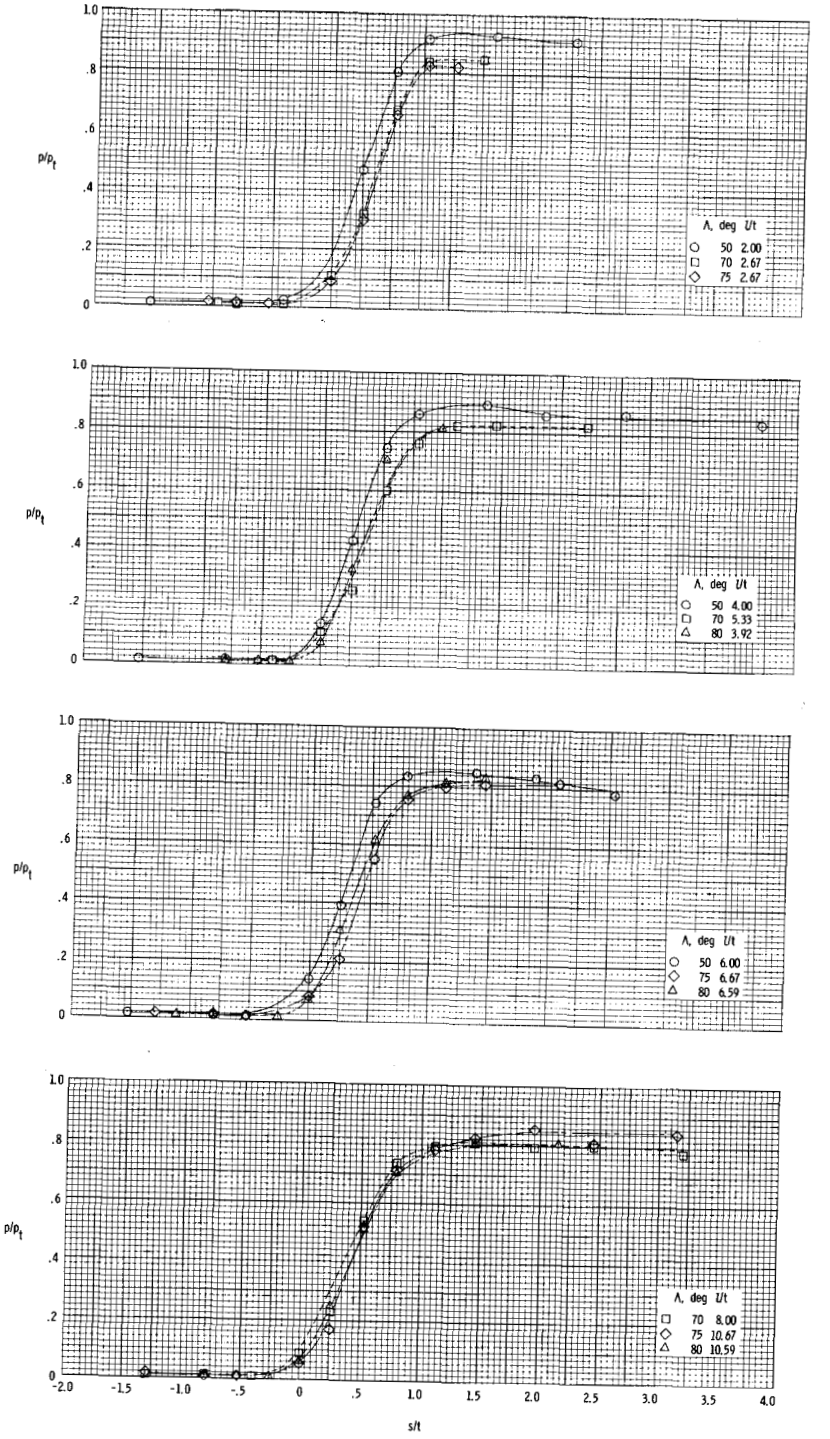

(b) $\alpha = 60°$.

Figure 5.- Continued.

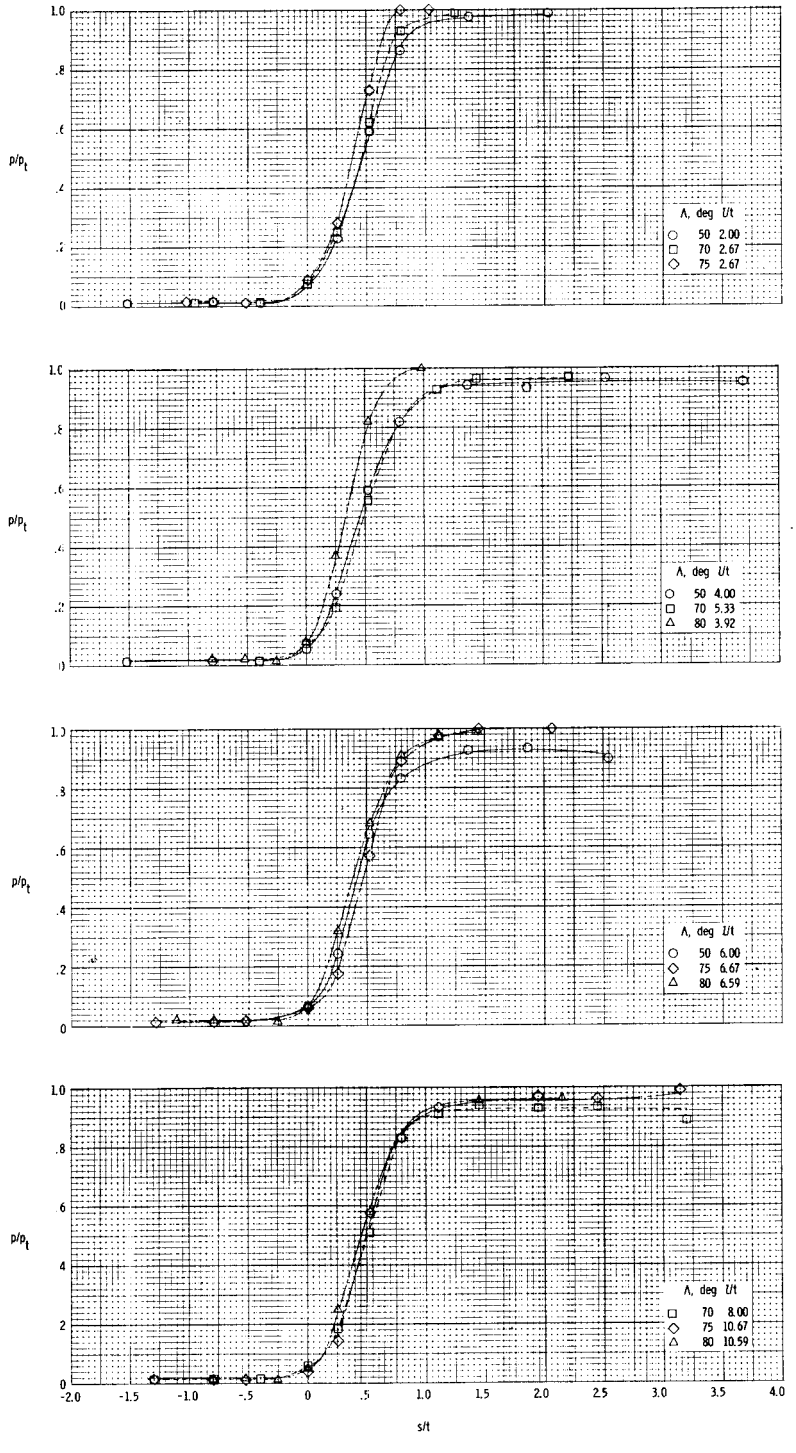

(c) $\alpha = 80^{\circ}$.

Figure 5.- Continued.

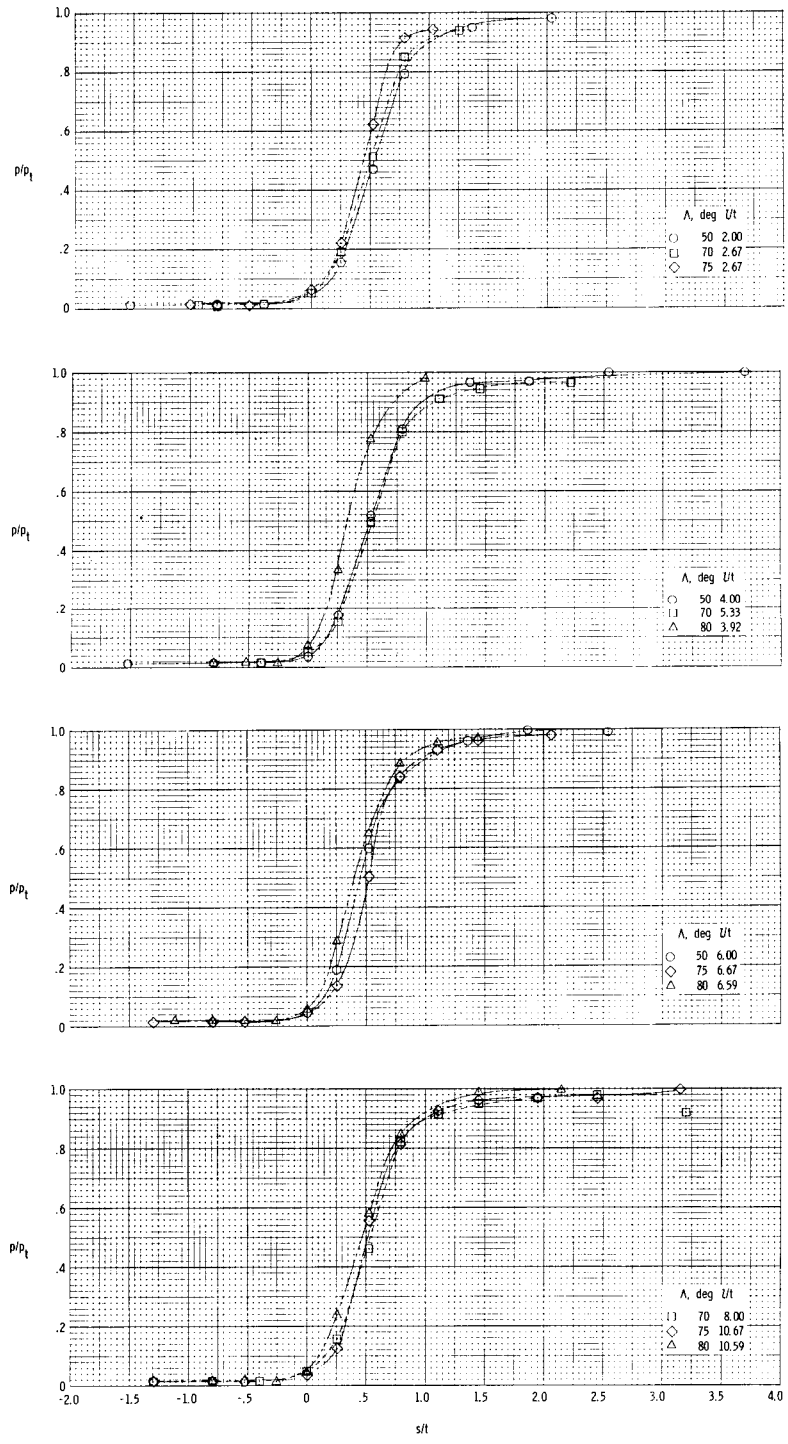

(d) $\alpha = 90^{\circ}$.

Figure 5.- Concluded.

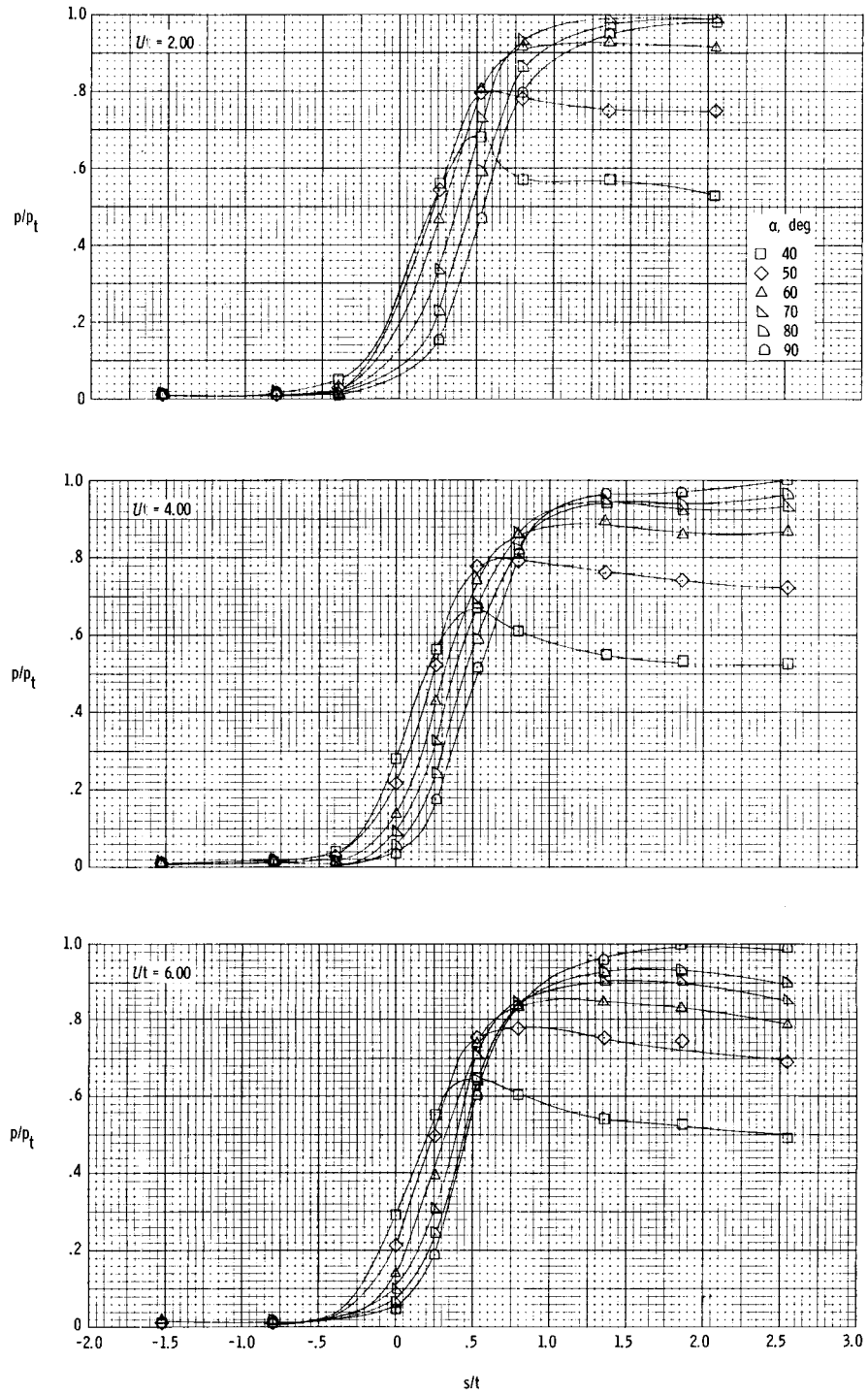

(a) $\Lambda = 50^\circ$.

Figure 6.- Effect of angle of attack on pressure distributions.

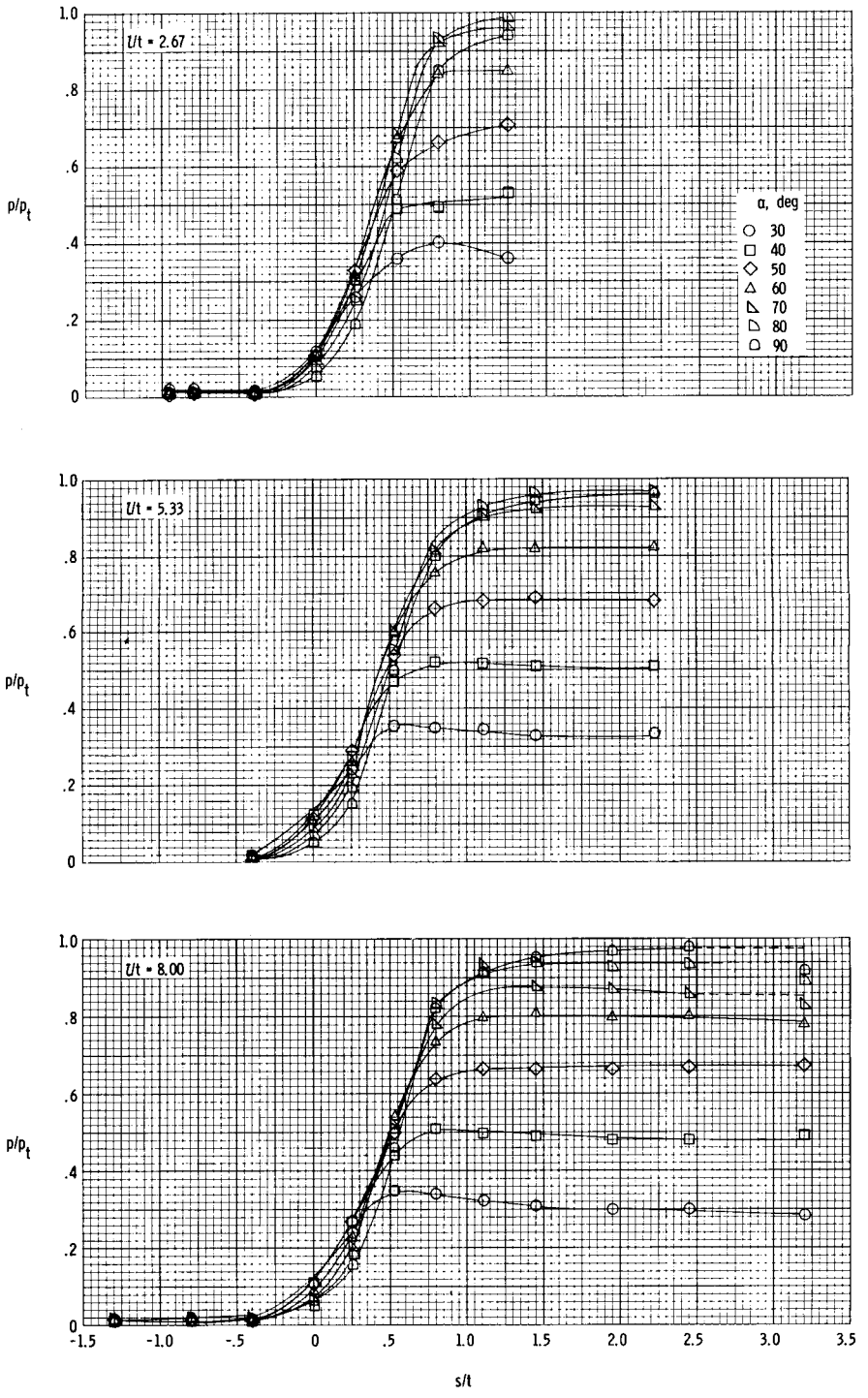

(b) $\Lambda = 70^{\circ}$.

Figure 6.- Continued.

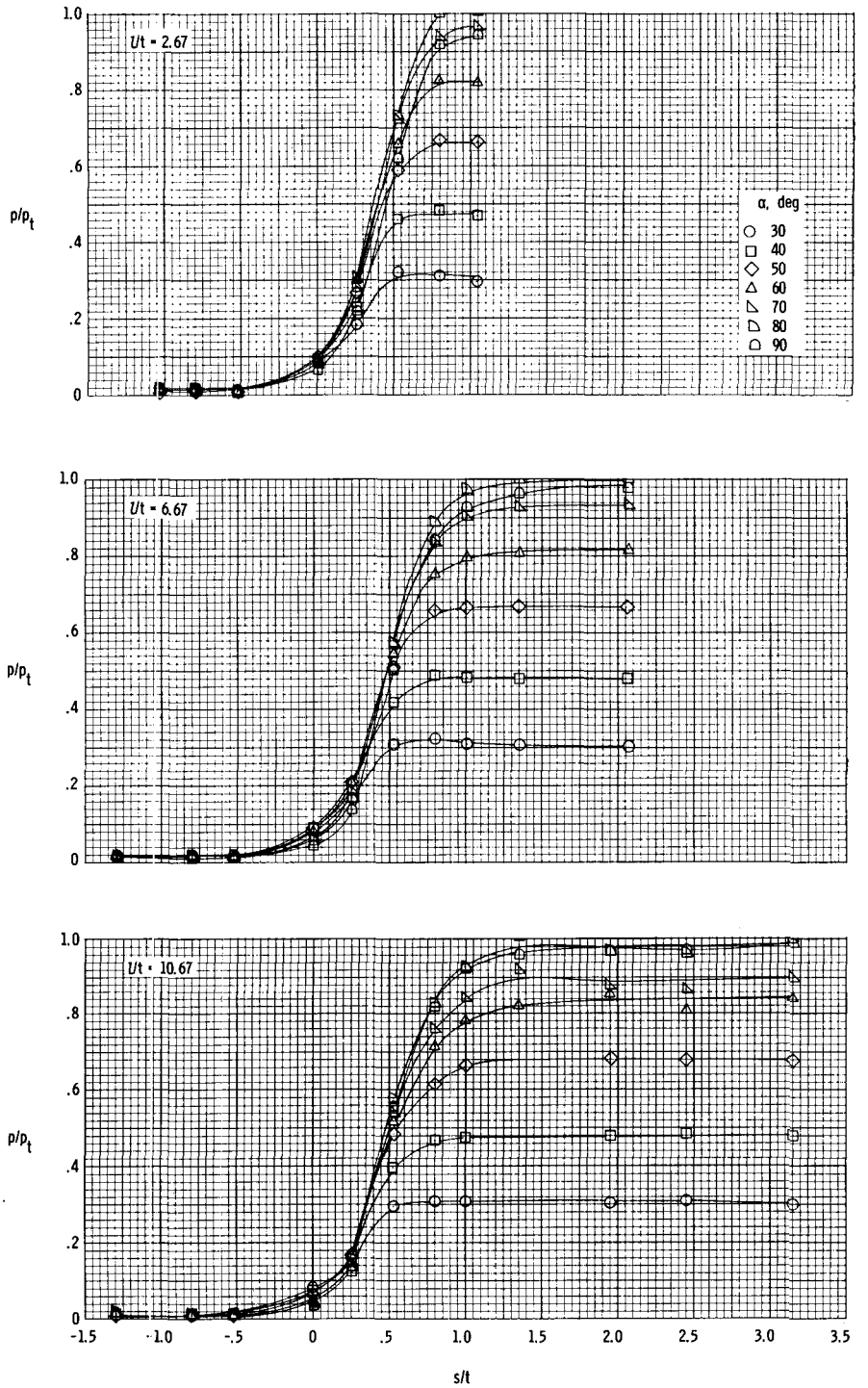

(c) $\Lambda = 75^{\circ}$.

Figure 6.- Continued.

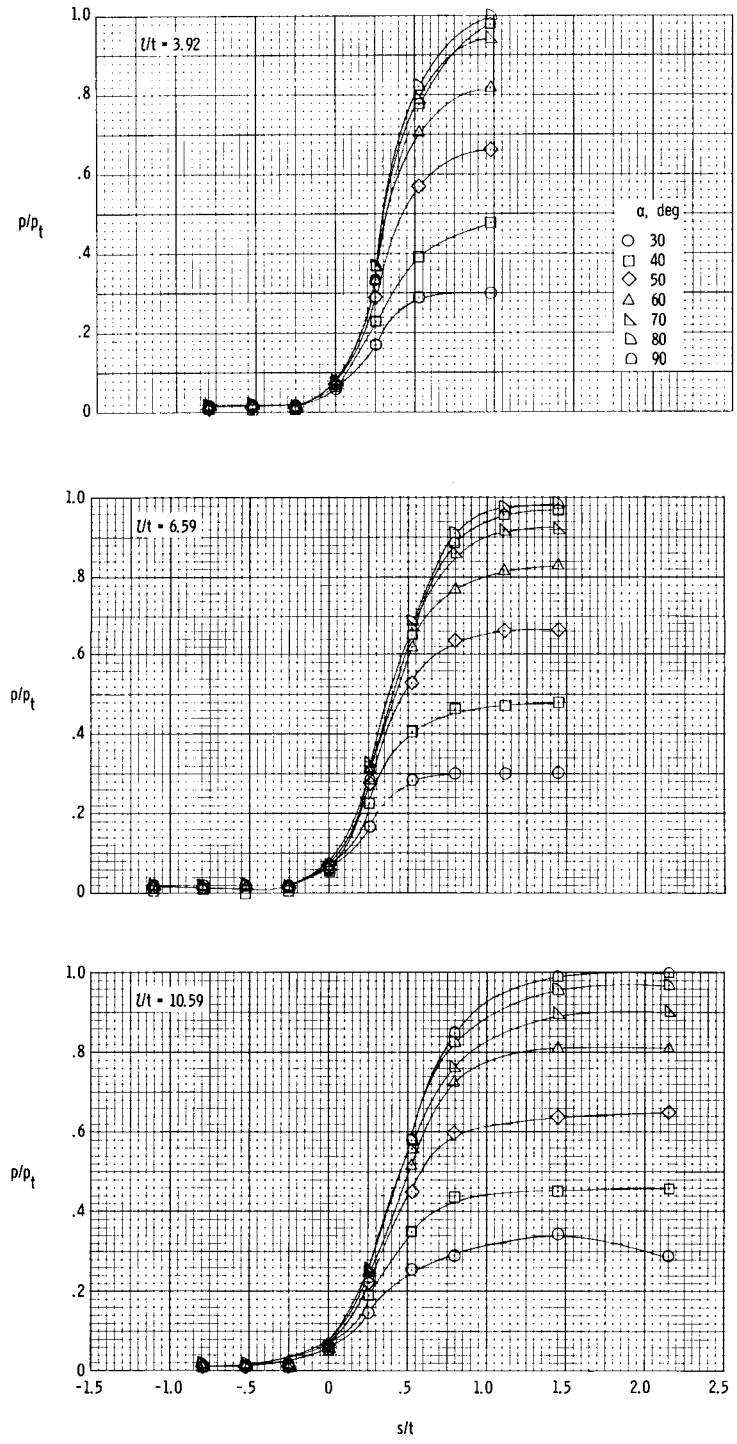

(d) $\Lambda = 80^{\circ}$.

Figure 6.- Concluded.

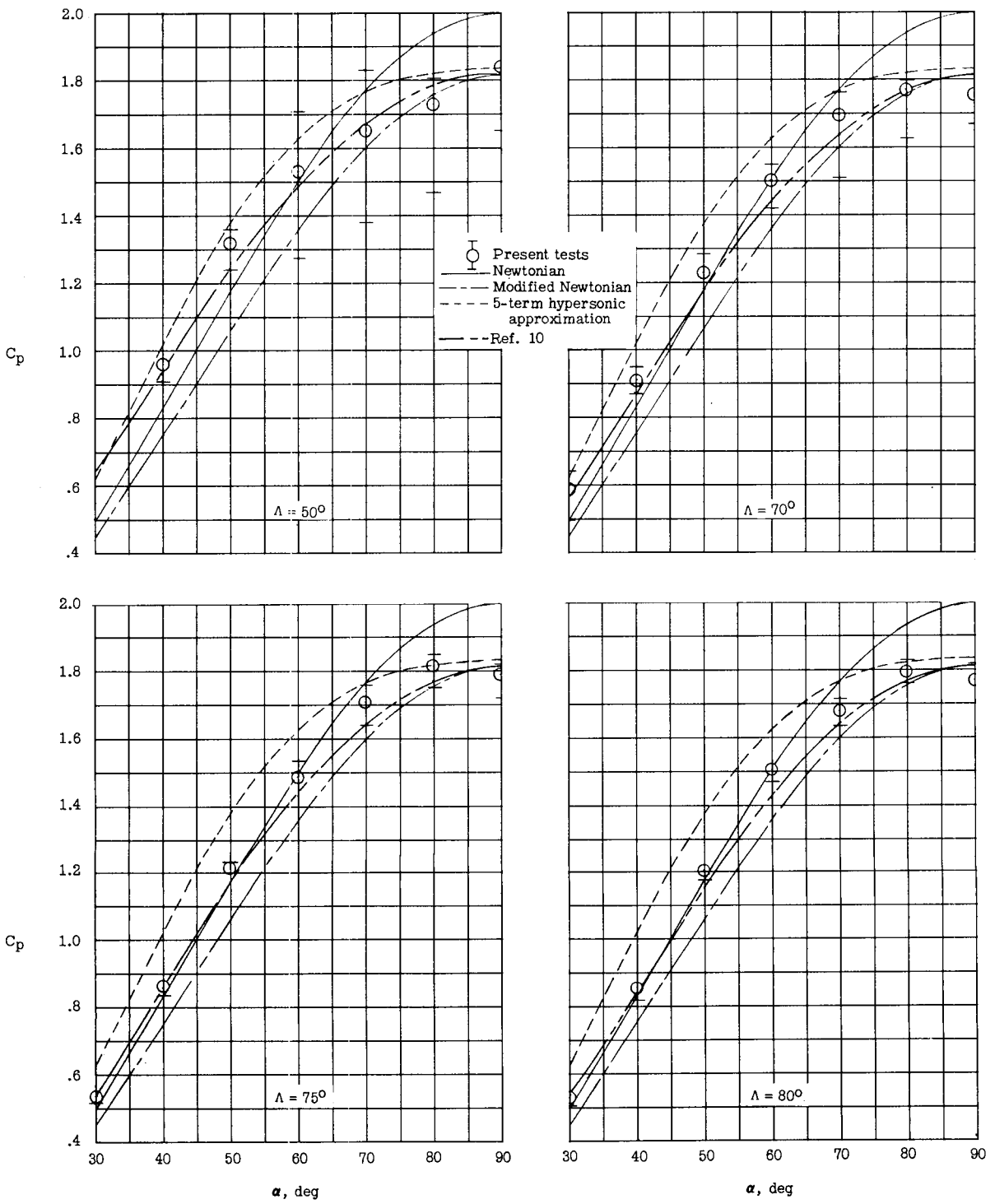

Figure 7.- Compilation of pressures measured on windward center line of blunt delta wings at angles of attack.

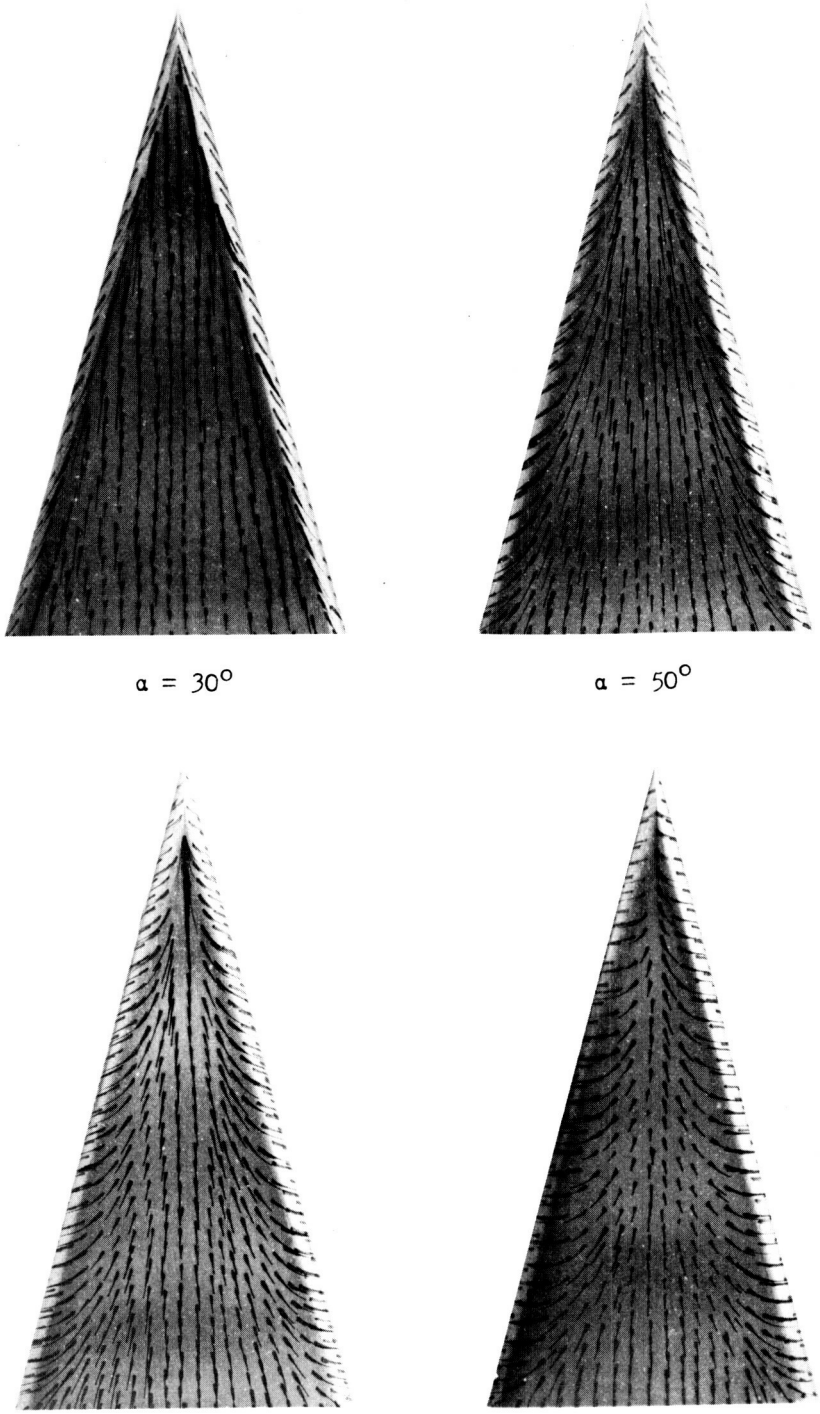

Figure 8.- Photographs of oil-flow patterns on a 75° sweep delta wing at various angles of attack.

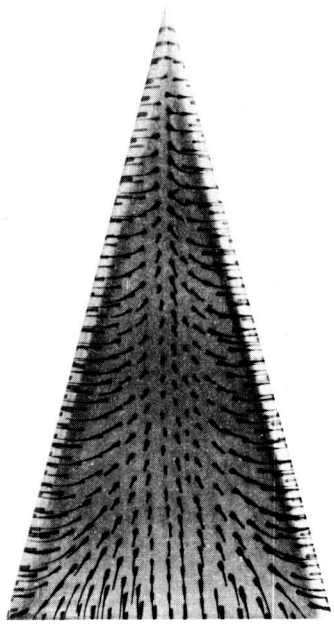

$\alpha = 75^{\circ}$

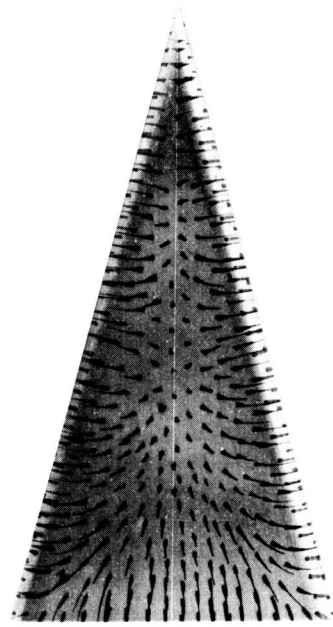

$\alpha = 80^{\circ}$

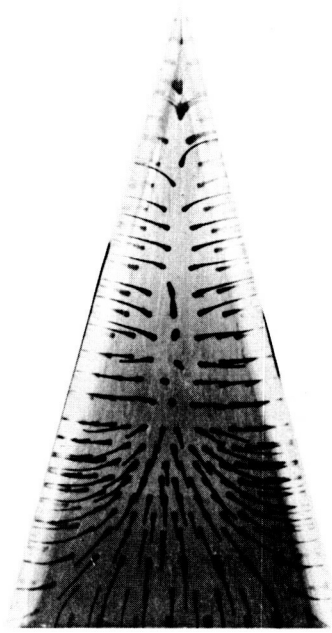

$\alpha = 85^{\circ}$

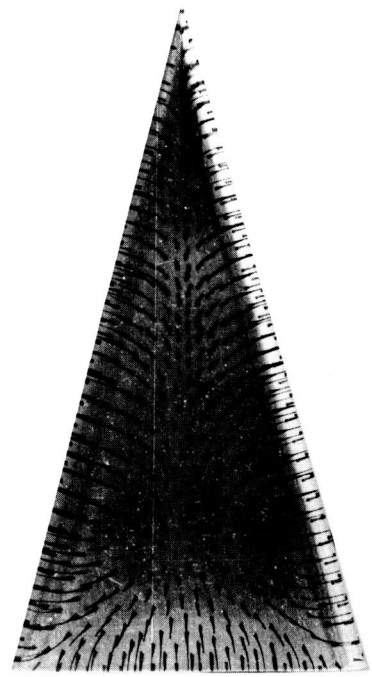

$\alpha = 90^{\circ}$

L-63-3107

Figure 8.- Concluded.